

**PARAMETER MATCHING USING ADAPTIVE
SYNCHRONIZATION OF CHUA'S CIRCUIT**

THESIS

**Submitted in Partial Fulfillment of
the Requirements for
the Degree of**

BACHELOR OF SCIENCE (Electrical Engineering)

at the

**POLYTECHNIC INSTITUTE OF NEW YORK
UNIVERSITY**

Valentin Siderskiy

January 2014

PARAMETER MATCHING USING ADAPTIVE SYNCHRONIZATION OF CHUA'S CIRCUIT

THESIS

Submitted in Partial Fulfillment of
the Requirements for
the Degree of

BACHELOR OF SCIENCE (Electrical Engineering)

at the

POLYTECHNIC INSTITUTE OF NEW YORK
UNIVERSITY

by

Valentin Siderskiy

January 2014

Advisor

Date

Department Head

Copy No. _____

Student ID# _____

Date

Vita

Valentin Siderskiy was born in Odessa, Ukraine, on August 25, 1987. He and his family immigrated to the United States in 1993. His interest in engineering began early on which led him to graduate from the Middlesex County Academy for Science, Mathematics and Engineering Technologies in Edison, NJ, in 2005. Afterwards, he started his undergraduate degree in electrical engineering at the Polytechnic Institute of NYU (NYU-Poly). While an undergraduate student, Valentin was vice-president of Eta Kappa Nu, member of Tau Beta Pi, and a member of the Honors College. Outside of his academic studies, he did a summer internship at the US Army, worked two years at Philips Research, and performed consulting work. In July 2007, Valentin started working at the Mechatronics Lab through the Summer Mechatronics Institute for Teachers (SUMMIT) program. This led him to work on chaotic systems until 2009 and then again from 2012 to 2013. His work at the Mechatronics lab was supported in part by the NY Space Grant: 48240-7887.

Acknowledgment

I would like to express my gratitude to my thesis advisor, Dr. Vikram Kapila. Working with him has taught me the value of independence and the value of one's own ideas. His patience and understanding is what made this research possible. His teachings proved to be more valuable than any of my other academic or interpersonal skills.

During my course of study, certain faculty and staff have been kind enough to display a personal interest. I would be lost without the advice and guidance of Ms. Ellen T. Daniels, Dr. Iraj M Kalkhoran, Ms. Rachel Jacobovits, Dr. Stephen Arnold, and Dr. Haldun Hadimioglu.

I would also like to use this opportunity to bring particular attention to faculty members who helped me bring my level of knowledge to a higher plane. These dedicated faculty not only brought enthusiasm and excitement into the classroom, but also raised expectations for the students. With every class I completed, not only did I learn the benchmark material, but I also came out a more learned person. Thank you, Dr. Franziska Berger and Dr. Farshad Khorrami.

I also thank Dr. Sang-Hoon Lee and Irina Igel as my fellow peers who gave me their time, attention, and knowledge at the Mechatronics Laboratory.

I am very fortunate to have so many good friends that are a positive influence. They are my greatest motivators. I thank Victoria Chen, Richard Kroon, Ivan Kharchenko, Ritchy Laurent, Dr. Lamia Iftekhhar, Srinivasa Chemudupati, and again Dr. Sang-Hoon Lee and Irina Igel.

Lastly, I would like to put the spotlight on my family. They have supported me in every way they could.

AN ABSTRACT

**PARAMETER MATCHING USING ADAPTIVE
SYNCHRONIZATION OF CHUA'S CIRCUIT**
by

Valentin Siderskiy

Advisor: Professor Vikram Kapila

**Submitted in Partial Fulfillment of the Requirements
for the Degree of Bachelor of Science (Electrical Engineering)**

January 2013

In this research, we develop an adaptive synchronization technique for parameter matching with chaotic persistent excitation (PE). Two Chua's oscillators, identical in every parameter except for one, are setup in a master/slave configuration where the slave's mismatched parameter is adaptable. Using Lyapunov functions and incorporating the presence of PE, adaptive control laws are designed to ensure exact parameter matching. One of the derived adaptive controllers is experimentally validated by using an adaptive inductor-gyrator composed of current feedback op-amps (CFOAs). The experimental results are compared to high-fidelity SPICE simulations, and performance of the adaptive controllers are compared over a wide range of parameters in MATLAB.

Contents

Vita	ii
Acknowledgment	iii
Abstract	iv
List of Figures	vi
List of Tables	viii
1 Introduction	1
2 System Model	3
2.1 Chua's Oscillator	3
2.2 Master/slave System	4
3 Adaptive Synchronization	5
3.1 Tuning \tilde{L}	5
3.2 Tuning C_2	8
4 Tuning \tilde{L} Implementation	10
4.1 Inductor-Gyrator	10
4.2 \tilde{L} Parameter Update	13
4.3 Experimental Setup	15
5 Experimental, SPICE, and MATLAB Results	18

<i>CONTENTS</i>	vi
5.1 Experimental Results	18
5.2 SPICE Simulation Results	24
5.3 MATLAB Simulation Results	29
5.4 Discussion	32
6 Conclusion	35
A TINA-TI SPICE Simulation 1 Schematic	36
B MATLAB-Simulink Simulation	37
B.1 MATLAB-Simulink	37
B.1.1 Run.m	37
B.2 Master Chua's Oscillator	39
B.3 Slave Chua's Oscillator	40
B.3.1 C_2 Adaptive Controller	40
B.3.2 Chua Diode	41
B.4 Bifurcation	41
B.4.1 BifurcationAnalysis.m	41
B.4.2 Simulink Diagram Called by BifurcationAnalysis.m	43
Bibliography	44

List of Figures

2.1	Master/slave Chua’s oscillator coupling.	4
4.1	(a) Current direction convention for the CFOA, (b) grounded version of the gyrator schematic from [Senani et al., 2009], and (c) modified version with a reciprocal r_{DS} relationship to impedance.	11
4.2	Schematic of master/slave Chua’s oscillator as constructed in the experiment.	12
4.3	Physical realization of \tilde{L} parameter update law. R_{Z2} is tuned manually to cancel AD633 DC offset.	13
4.4	Experimental setup: (a) close up of circuitry and data acquisition device, (b) full setup when switch SW1 is closed, and (c) full setup when switch SW1 is open.	17
5.1	Experiment 1	20
5.2	Experiment 2	21
5.3	Experiment 3	22
5.4	Experiment 4	23
5.5	SPICE Simulation 1	25
5.6	SPICE Simulation 2	26
5.7	SPICE Simulation 3	27
5.8	SPICE Simulation 4	28
5.9	Chua’s oscillator bifurcation diagram along C_1	30
5.10	MATLAB Simulation 1: Adapting for \tilde{L}	31
5.11	MATLAB Simulation 2: Adapting for \tilde{C}_2	31
5.12	MATLAB Simulation 3: Adapting for \tilde{L} with tolerances.	32

5.13	MATLAB Simulation 4: Adapting for \tilde{C}_2 with tolerances.	32
5.14	Demonstration of four step tuning methodology.	34
A.1	TINA-TI Schematic of SPICE Simulation 1.	36
B.1	Simulink model Adapte_Synch_C2_IdealChua.mdl.	39
B.2	Simulink model of master Chua's oscillator.	39
B.3	Simulink model of slave Chua's oscillator with adaptive C_2	40
B.4	Simulink Model of C_2 Adaptive Controller.	40
B.5	Simulink model used to generate bifurcation data.	43

List of Tables

4.1	Constant Components	16
5.1	Experiment 1	20
5.2	Experiment 2	21
5.3	Experiment 3	22
5.4	Experiment 4	23
5.5	SPICE Simulation 1	25
5.6	SPICE Simulation 2	26
5.7	SPICE Simulation 3	27
5.8	SPICE Simulation 4	28
5.9	MATLAB Simulation Parameters	29

Chapter 1

Introduction

Leon Chua is credited with developing one of the simplest to construct chaotic circuits [Matsumoto, 1984], which is now termed as the Chua's circuit. The basic properties of chaotic systems, specifically, sensitivity to initial conditions and dense topology, intuitively suggest that in the physical world a chaotic system is too sensitive and its behavior is too complex to predict or match. Note that, in non-chaotic systems such problems are frequently solved by using an array of tools from the stability and control theory. Moreover, the experiment of Pecora and Carroll [1990] showed that we can not only build chaotic systems but also go beyond intuition and work with chaos, for example, to cause one chaotic system to mimic another chaotic system by using stability and control theory. Since Pecora and Carroll [1990], synchronization of chaotic systems has received considerable attention from the research community. Naturally, the works of Matsumoto [1984] and Pecora and Carroll [1990] led to synchronization of two Chua's circuits [Chua et al., 1992].

Synchronization of Chua's oscillators along with parameter adaptation has been considered since 1996 [Chua et al., 1996; Kozlov et al., 1996; Parlitz and Kocarev, 1996; Wu et al., 1996]. For example, Wu et al. [1996] used a Lyapunov-based approach to adapt parameters relating to the Chua's diode, while Chua et al. [1996] used an adaptive control technique introduced by Huberman and Lumer [1990] and John and Amritkar [1994] to adapt mismatched parameters for the rest of the circuit. These two papers complement one-another by collectively providing an adaptive control scheme for every parameter in the Chua's oscillator. Theoretical result of Wu et al. [1996] showed asymptotic stability for the error dynamics of the states of the Chua's oscillator but not for the adaptive parameters. Despite this, the adaptive parameters were shown to asymptotically converge in simulation results and it was conjectured that "parameters match when the dynamics are very rich" [Wu et al., 1996]. These rich dynamics are commonly referred to as PE [Lian et al., 2002] and we will employ this terminology later in the thesis. It is useful to note that Chua et al. [1996] and [Wu et al., 1996] gave simple controllers that were later compared in Wu [2002].

Numerous other papers have considered adaptive synchronization control for Chua's oscillators including adaptive observer design [Franks and Markov, 1997; Frandkov et al., 2000; Lian et al., 2002], parameter identification [Zhou et al., 2006], synchronization of different chaotic systems using

adaptive control [Femat et al., 2000; Wagg, 2002], adaptive backstepping [Ge and Wang, 2000; Haeri and Khademian, 2006], and H_∞ adaptive synchronization [Koofigar et al., 2011]. Many of these works are theoretical in nature and are difficult to realize experimentally while others may not yield exact parameter matching [Bowong et al., 2006]. To render adaptive parameter chaotic circuits closer to physical realization Xiao and Cao [2009] have provided SPICE simulations and Jin et al. [2012] have suggested circuit schematics.

Adaptive synchronization of Chua’s oscillators can be categorized in two parts, adapting the control coupling between the two circuits [Chua et al., 1996; Lin et al., 2005; Liu and Chen, 2010; Naseh and Haeri, 2005] and adapting one or more parameters of the Chua’s oscillators. Both adaptive synchronization approaches have been *digitally* implemented for secure communication applications. The first approach consisting of control coupling adaptation is used to account for changes in signal strength [Xie et al., 2002; Zhu and Cui, 2010], while the second approach consisting of chaotic circuit parameter adaptation introduces deliberate changes in the parameters as a way to send binary messages as a “key”. Chua et al. [1996] have provided an experimental validation of synchronization with adaptive control coupling where the entire system is realized using *analog* circuitry. To the best of our knowledge, the present work is the first one to provide an experimental validation of synchronization with adaptive parameter tuning for the Chua’s oscillator where the entire system is realized using analog circuitry. Chaotic systems may be exploited in a variety of applications including sensing [Brown et al., 1992], damage detection [Nichols et al., 2003; Dubey and Kapila, 2012], signal transmission [Corron and Hahs, 1997], etc. Other works related specifically to adaptive control of chaotic systems geared towards physical implementation and practical applications include Aida and Davis [1994]; Cohen et al. [2010], and Ravoori et al. [2009] for electro-optic applications and Ge and Lin [2003] for electro-mechanical applications.

The focus of this research is to experimentally demonstrate adaptive synchronization with parameter matching. We use the Lyapunov function technique of Wu et al. [1996] to create parameter update laws for parameters \tilde{L} and \tilde{C}_2 of Chua’s oscillator in Figure 2.1. The derived result for tuning \tilde{L} is realized with analog circuit components and \tilde{L} is continuously updated by using a voltage-controlled inductor-gyrator made up of CFOAs described in Chapter 4.

This thesis is organized as follows. In Chapter 2, we present the mathematical model used for our master/slave Chua’s oscillator. Next, in Chapter 3, we provide adaptive control laws and show proof of stability using Lyapunov functions. In Chapter 4, we provide physical realization of one of the adaptive controller circuit and the inductor-gyrator circuit. In Chapter 5, we provide a series of results including experimental results, SPICE simulations with ideal passive component values, SPICE simulations with tolerances in passive component values, and MATLAB simulations that provide performance measures of the adaptive controllers over a wide span of L and C_2 . Finally, in Chapter 6, we provide some concluding remarks.

Chapter 2

System Model

2.1 Chua's Oscillator

In this research, adaptive controllers are designed to tune parameters of the Chua's oscillator shown in Figure 2.1. Various parameters of a Chua's oscillator include L as a linear inductor, R and R_0 as linear resistors, C_1 and C_2 as linear capacitors, and others that correspond to the Chua's diode. The state equations of the Chua's oscillator are given by

$$\frac{dv_1}{dt} = \frac{1}{C_1} \left(G(v_2 - v_1) - g(v_1) \right), \quad (2.1a)$$

$$\frac{dv_2}{dt} = \frac{1}{C_2} \left(G(v_1 - v_2) + i_L \right), \quad (2.1b)$$

$$\frac{di_L}{dt} = \frac{1}{L} (-v_2 - R_0 i_L), \quad (2.1c)$$

where v_1 , v_2 , and i_L are voltage across C_1 , voltage across C_2 , and current through L , respectively, and G is the conductance of the resistor R ($G \triangleq \frac{1}{R}$). Furthermore $g(\cdot)$ is the nonlinear voltage-current ($v-i$) characteristic of the Chua's diode described by

$$g(v_R) = \begin{cases} G_b v_R + (G_b - G_a) E_1, & \text{if } v_R \leq -E_1 \\ G_a v_R, & \text{if } |v_R| < E_1 \\ G_b v_R + (G_a - G_b) E_1, & \text{if } v_R \geq E_1 \end{cases}, \quad (2.2)$$

where G_a , G_b , and E_1 are known real constants that satisfy $G_b < G_a < 0$ and $E_1 > 0$.

2.2 Master/slave System

The adaptive control framework of this research considers a unidirectional coupling between a master Chua's oscillator and a slave Chua's oscillator. Specifically, the master Chua's oscillator operates autonomously whereas the slave Chua's oscillator synchronizes its states to the states of the master oscillator. A depiction of this configuration is displayed in Figure 2.1 where it is assumed that the following parameters of the master and slave Chua's oscillator are matched, $\tilde{R} = R$, $\tilde{R}_0 = R_0$, $\tilde{C}_1 = C_1$. The master Chua's oscillator state equations are equivalent to (2.1) while the slave Chua's oscillator state equations are given by

$$\frac{d\tilde{v}_1}{dt} = \frac{1}{C_1} \left(G(\tilde{v}_2 - \tilde{v}_1) - g(\tilde{v}_1) + G_{u_1}(v_{u_1} - \tilde{v}_1) \right), \quad (2.3a)$$

$$\frac{d\tilde{v}_2}{dt} = \frac{1}{\tilde{C}_2} \left(G(\tilde{v}_1 - \tilde{v}_2) + \tilde{i}_L \right), \quad (2.3b)$$

$$\frac{d\tilde{i}_L}{dt} = \frac{1}{\tilde{L}} (-\tilde{v}_2 - R_0 \tilde{i}_L), \quad (2.3c)$$

where $v_{u_1} = v_1$ since it is the output of a voltage follower op-amp and G_{u_1} is the conductance of the coupling resistor R_{u_1} in Figure 2.1 ($G_{u_1} \triangleq \frac{1}{R_{u_1}}$). Note that \tilde{C}_2 and \tilde{L} are tunable parameters for which we provide adaptive parameter update laws in Chapter 3.

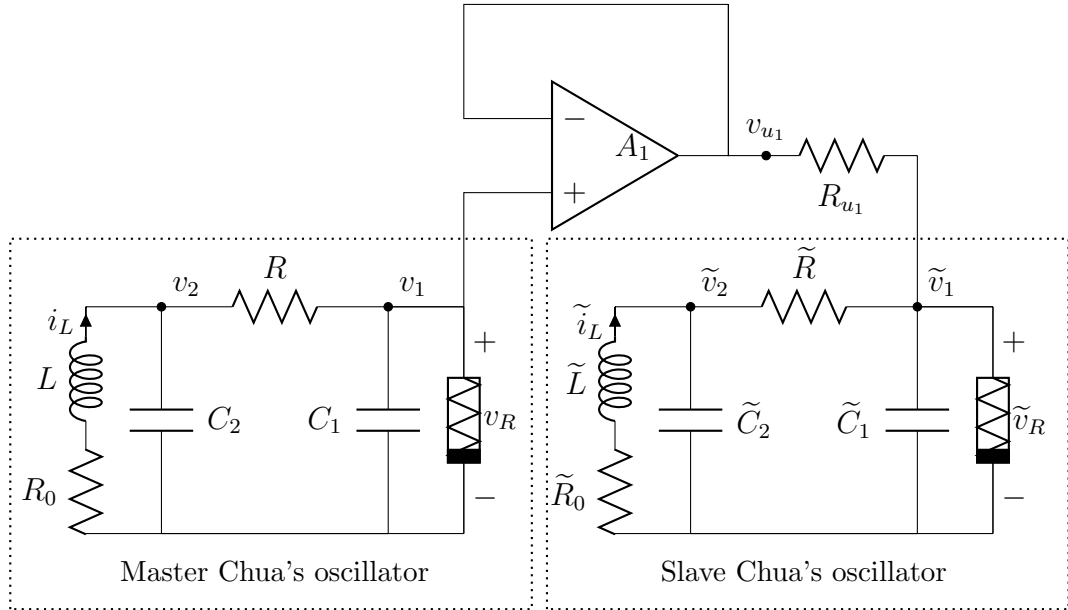


Figure 2.1: Master/slave Chua's oscillator coupling.

Chapter 3

Adaptive Synchronization

Given two Chua's oscillators with unidirectional coupling and one mismatched parameter, we design an adaptive controller to synchronize the two oscillators and tune the slave oscillator's parameter to the master oscillator's parameter. Using the ideal Chua's oscillator model (2.1), two cases are considered to tune either \tilde{L} or \tilde{C}_2 .

3.1 Tuning \tilde{L}

In a master/slave configuration, the master Chua's oscillator is described as in (2.1). For the slave Chua's oscillator, when capacitance \tilde{C}_2 matches the master oscillator's parameter C_2 ($\tilde{C}_2 = C_2$) and inductance \tilde{L} is the tunable mismatched parameter, (2.3) specializes to

$$\frac{d\tilde{v}_1}{dt} = \frac{1}{C_1} \left(G(\tilde{v}_2 - \tilde{v}_1) - g(\tilde{v}_1) + u_1 \right), \quad (3.1a)$$

$$\frac{d\tilde{v}_2}{dt} = \frac{1}{C_2} \left(G(\tilde{v}_1 - \tilde{v}_2) + \tilde{i}_L \right), \quad (3.1b)$$

$$\frac{d\tilde{i}_L}{dt} = \frac{1}{\tilde{L}} \left(-\tilde{v}_2 - R_0 \tilde{i}_L \right), \quad (3.1c)$$

where $u_1 \triangleq G_{u_1}(v_1 - \tilde{v}_1)$.

Subtracting (2.1) from (3.1) produces the error dynamics

$$\dot{e}_{v_1} = \frac{1}{C_1} \left(G(e_{v_2} - e_{v_1}) - c(\tilde{v}_1, v_1) e_{v_1} + u_1 \right), \quad (3.2a)$$

$$\dot{e}_{v_2} = \frac{1}{C_2} \left(G(e_{v_1} - e_{v_2}) + e_{i_L} \right), \quad (3.2b)$$

$$\dot{e}_{i_L} = \frac{1}{\tilde{L}} (-\tilde{v}_2 - R_0 \tilde{i}_L) + \frac{1}{L} (v_2 + R_0 i_L), \quad (3.2c)$$

where $e_{v_1} \triangleq \tilde{v}_1 - v_1$, $e_{v_2} \triangleq \tilde{v}_2 - v_2$, and $e_{i_L} \triangleq \tilde{i}_L - i_L$ are the error states. Moreover, it is easy to show that $g(\tilde{v}_1) - g(v_1) = c(\tilde{v}_1, v_1)e_{v_1}$ where $c(\tilde{v}_1, v_1)$ is bounded by the constraints $G_a \leq c(\tilde{v}_1, v_1) \leq G_b < 0$ [Hegazi et al., 2002].

Next, let the control law for u_1 be characterized as

$$u_1 = -G_{u_1} e_{v_1} \quad (3.3)$$

and let the parameter update law be given by

$$\frac{d}{dt} \left(\frac{1}{\tilde{L}} \right) = \gamma e_{i_L} (\tilde{v}_2 + R_0 \tilde{i}_L), \quad (3.4)$$

where γ is a positive constant.

Theorem 1. *The two Chua's oscillators (2.1) and (3.1) will synchronize and the parameter \tilde{L} will converge to some constant under the control law (3.3) and the parameter update law (3.4) if the master system (2.1) remains on the trajectory of its chaotic attractor and G_{u_1} is chosen to satisfy the following inequality*

$$G_{u_1} > \frac{1}{2}G - G_a. \quad (3.5)$$

Proof. Let $e_\rho \triangleq \frac{1}{\tilde{L}} - \frac{1}{L}$, then the dynamics of e_ρ is

$$\dot{e}_\rho = \frac{d}{dt} \left(\frac{1}{\tilde{L}} \right), \quad (3.6)$$

since L is constant. Consider a candidate Lyapunov function V adopted from Wu et al. [1996]

$$V(e_{v_1}, e_{v_2}, e_{i_L}, e_\rho) = \frac{C_1}{4} e_{v_1}^2 + \frac{C_2}{2} e_{v_2}^2 + \frac{L}{2} e_{i_L}^2 + \frac{L}{2\gamma} e_\rho^2. \quad (3.7)$$

Note that V is a positive definite function. Moreover, by computing the time derivative of V we obtain

$$\dot{V}(e_{v_1}, e_{v_2}, e_{i_L}, e_\rho) = \frac{C_1}{2} e_{v_1} \dot{e}_{v_1} + C_2 e_{v_2} \dot{e}_{v_2} + L e_{i_L} \dot{e}_{i_L} + \frac{L}{\gamma} e_\rho \dot{e}_\rho. \quad (3.8)$$

Substituting (3.2) into (3.8) produces

$$\begin{aligned} \dot{V}(e_{v_1}, e_{v_2}, e_{i_L}, e_\rho) &= \frac{e_{v_1}}{2} \left(G(e_{v_2} - e_{v_1}) - c(\tilde{v}_1, v_1)e_{v_1} + u_1 \right) + e_{v_2} \left(G(e_{v_1} - e_{v_2}) + e_{i_L} \right) \\ &\quad + L e_{i_L} \left(-\frac{1}{\tilde{L}} (\tilde{v}_2 + R_0 \tilde{i}_L) + \frac{1}{L} (v_2 + R_0 i_L) \right) + \frac{L}{\gamma} e_\rho \dot{e}_\rho. \end{aligned} \quad (3.9)$$

Next, by adding and subtracting $e_{i_L}(\tilde{v}_2 + R_0 \tilde{i}_L)$ to (3.9) and simplifying the resulting equation

yields

$$\begin{aligned} \dot{V}(e_{v_1}, e_{v_2}, e_{i_L}, e_\rho) = & - \left(\frac{G}{2} + \frac{c(\tilde{v}_1, v_1)}{2} \right) e_{v_1}^2 - G e_{v_2}^2 - R_0 e_{i_L}^2 + \frac{3}{2} G e_{v_1} e_{v_2} \\ & + \frac{e_{v_1} u_1}{2} + e_\rho L \left(\frac{1}{\gamma} \dot{e}_\rho - e_{i_L} (\tilde{v}_2 + R_0 \tilde{i}_L) \right). \end{aligned} \quad (3.10)$$

By substituting the control law (3.3) and the parameter update law (3.4), we can show that

$$\dot{V}(e_{v_1}, e_{v_2}, e_{i_L}, e_\rho) = - \left(\frac{G + c(\tilde{v}_1, v_1) + G_{u_1}}{2} \right) e_{v_1}^2 - G e_{v_2}^2 - R_0 e_{i_L}^2 + \frac{3}{2} G e_{v_1} e_{v_2}. \quad (3.11)$$

Moreover, by using the bound for $c(\tilde{v}_1, v_2)$, we now obtain

$$\dot{V}(e_{v_1}, e_{v_2}, e_{i_L}, e_\rho) \leq - \left(\frac{G + G_a + G_{u_1}}{2} \right) e_{v_1}^2 - G e_{v_2}^2 - R_0 e_{i_L}^2 + \frac{3}{2} G e_{v_1} e_{v_2}. \quad (3.12)$$

Next, by defining the notation $e \triangleq [e_{v_1} \ e_{v_2} \ e_{i_L} \ e_\rho]^T$ we can rewrite (3.12) as $\dot{V}(e_{v_1}, e_{v_2}, e_{i_L}, e_\rho) \leq -e^T P e$ where

$$P \triangleq \begin{pmatrix} \frac{1}{2}(G + G_a + G_{u_1}) & -\frac{3}{4}G & 0 & 0 \\ -\frac{3}{4}G & G & 0 & 0 \\ 0 & 0 & R_0 & 0 \\ 0 & 0 & 0 & 0 \end{pmatrix}. \quad (3.13)$$

Note that matrix P is positive-semidefinite if $G_{u_1} > \max(-3G - G_a, \frac{1}{8}G - G_a)$, which is automatically satisfied due to (3.5). Next, after substituting (3.3) into (3.2), adding and subtracting $\frac{1}{L}(v_2 + R_0 i_L)$ to and from (3.2c), and manipulating the resulting equations, we can represent the error dynamics as follows

$$\begin{aligned} \dot{e}_{v_1} &= \frac{1}{C_1} \left(G(e_{v_2} - e_{v_1}) - c(\tilde{v}_1, v_1)e_{v_1} - G_{u_1}e_{v_1} \right), \\ \dot{e}_{v_2} &= \frac{1}{C_2} \left(G(e_{v_1} - e_{v_2}) + e_{i_L} \right), \\ \dot{e}_{i_L} &= -e_\rho(v_2 + R_0 i_L) + \frac{1}{L}(-e_{v_2} - R_0 e_{i_L}). \end{aligned} \quad (3.14)$$

It now follows that $e = 0$ is an equilibrium point of (3.6) and (3.14). Since V is a positive and decrescent function and \dot{V} is negative semidefinite, it follows that the equilibrium point ($e = 0$) of the system (3.6) and (3.14) is uniformly stable, i.e., $e_{v_1}(t), e_{v_2}(t), e_{i_L}(t)$, and $e_\rho(t) \in L_\infty$.

Next, by using the inequality $pq < \frac{1}{2}p^2 + \frac{1}{2}q^2$, we can show that

$$\dot{V} < - \left(\frac{G + G_a + G_{u_1}}{2} \right) e_{v_1}^2 - G e_{v_2}^2 - R_0 e_{i_L}^2 + \frac{3}{4} G e_{v_1}^2 + \frac{3}{4} G e_{v_2}^2, \quad (3.15)$$

which simplifies to

$$\dot{V} < - \left(-\frac{1}{4}G + \frac{1}{2}G_a + \frac{1}{2}G_{u_1} \right) e_{v_1}^2 - \frac{1}{4}G e_{v_2}^2 - R_0 e_{i_L}^2. \quad (3.16)$$

From (3.5) and (3.16) we know that $e_{v_1}^2(t), e_{v_2}^2(t), e_{i_L}^2(t)$ are integrable with respect to time, i.e., $e_{v_1}(t), e_{v_2}(t), e_{i_L}(t) \in L_2$ (note that e_ρ may or may not be in L_2).

Note that if the master oscillator (2.1) remains on its chaotic trajectory, the states of the master system are bounded. In this case, $v_2, i_L \in L_\infty$ and it follows from (3.14) that $\dot{e}_{v_1}(t), \dot{e}_{v_2}(t), \dot{e}_{i_L}(t) \in L_\infty$. Next, by Barbalat's lemma, for any initial condition $e_{v_1}(t), e_{v_2}(t), e_{i_L}(t) \rightarrow 0$ as $t \rightarrow \infty$. This implies that Chua systems (2.1) and (3.1) will synchronize. \square

Remark 1. Note that the results of Theorem 1 are also applicable if the Chua's oscillator is on a periodic trajectory. As long as the attractor of the Chua's oscillator is bounded, the results of Theorem 1 hold.

Remark 2. When the trajectories of (2.1) are driven on a chaotic attractor, its states will satisfy the qualities of PE as discussed in Lian et al. [2002]; Narendra and Annaswamy [2005]; and Sastry and Bodson [2011] and $\tilde{L}(t) \rightarrow L(t)$ as $t \rightarrow \infty$. Further evidence of $\tilde{L}(t) \rightarrow L(t)$ as $t \rightarrow \infty$ is provided via simulation and experimental results in the sequel.

Remark 3. Equation (3.16) illustrates the importance of parameter R_0 to ensure that $e_{i_L} \in L_2$. In literature dealing with experimental implementation of Chua's oscillator, R_0 is usually considered as a parasitic resistance and is often ignored [Chua, 1994; Kilic, 2010]. In this work, we deliberately include R_0 to achieve our formal stability result.

3.2 Tuning C_2

In a similar manner as in the Chapter 3.1, the master Chua's oscillator is described in (2.1). For the slave Chua's oscillator, when inductance \tilde{L} matches the master oscillator's parameter L ($\tilde{L} = L$) and capacitance \tilde{C} is the tunable mismatched parameter, (2.3) specializes to

$$\frac{d\tilde{v}_1}{dt} = \frac{1}{C_1} \left(G(\tilde{v}_2 - \tilde{v}_1) - g(\tilde{v}_1) + u_1 \right), \quad (3.17a)$$

$$\frac{d\tilde{v}_2}{dt} = \frac{1}{\tilde{C}_2} \left(G(\tilde{v}_1 - \tilde{v}_2) + \tilde{i}_L \right), \quad (3.17b)$$

$$\frac{d\tilde{i}_L}{dt} = \frac{1}{\tilde{L}} \left(-\tilde{v}_2 - R_0 \tilde{i}_L \right). \quad (3.17c)$$

Subtracting (2.1) from (3.17) produces, the error dynamics

$$\dot{e}_{v_1} = \frac{1}{C_1} \left(G(e_{v_2} - e_{v_1}) - c(\tilde{v}_1, v_1)e_{v_1} + u_1 \right), \quad (3.18a)$$

$$\dot{e}_{v_2} = \frac{1}{\tilde{C}_2} \left(G(\tilde{v}_1 - \tilde{v}_2) + \tilde{i}_L \right) - \frac{1}{C_2} \left(G(v_1 - v_2) + i_L \right), \quad (3.18b)$$

$$\dot{e}_{i_L} = \frac{1}{L} (-e_{v_2} - R_0 e_{i_L}). \quad (3.18c)$$

Next, let the control law for u_1 be characterized as in (3.3) and let the parameter update law be given by

$$\frac{d}{dt} \left(\frac{1}{\tilde{C}_2} \right) = -\eta e_{v_2} \left(G(\tilde{v}_1 - \tilde{v}_2) + \tilde{i}_L \right), \quad (3.19)$$

where η is a positive constant.

Theorem 2. *The two Chua's oscillators (2.1) and (3.17) will synchronize and the parameter \tilde{C}_2 will converge to some constant under the control law (3.3) and the parameter update law (3.19) if the master system (2.1) remains on the trajectory of its chaotic attractor and G_{u_1} is chosen to satisfy (3.5).*

Proof. Theorem 2 can be proved in a similar manner as Theorem 1 using the following candidate Lyapunov function

$$V(e_{v_1}, e_{v_2}, e_{i_L}, e_\pi) = \frac{C_1}{4} e_{v_1}^2 + \frac{C_2}{2} e_{v_2}^2 + \frac{L}{2} e_{i_L}^2 + \frac{C_2}{2\eta} e_\pi^2, \quad (3.20)$$

where $e_\pi \triangleq \frac{1}{\tilde{C}_2} - \frac{1}{C_2}$. □

Chapter 4

Tuning \tilde{L} Implementation

Over the years, several variations of the Chua's oscillators have been developed [Kilic, 2010]. Similarly, master/slave coupling between two Chua's oscillators for state v_1 (and v_2) is easily achievable with just one resistor and one op-amp (Figure 2.1). However, measuring and controlling the state i_L is not as trivial. Therefore variations of inductorless implementations of Chua's oscillators have been developed [Kilic, 2010]. This research implements the adaptive controller presented in Section 3.1 which tunes the parameter \tilde{L} to L . This section describes the circuitry required for this task and it includes *i*) an inductorless implementation of Chua's oscillator using an inductor-gyrator and *ii*) a physical realization of the adaptive parameter update law for \tilde{L} .

4.1 Inductor-Gyrator

To achieve adaptive control of master/slave Chua's oscillators with the tuning of the parameter \tilde{L} , we begin by recognizing that the parameter update law (3.4) is the rate of change for the **reciprocal** of the inductance (\tilde{L}) and it requires the measurement of i_L , \tilde{i}_L and \tilde{v}_2 . The use of CFOAs has led to Chua's oscillator implementations with access to i_L measurements [Kilic, 2010]. Each CFOA is a four port device in which the voltages on and currents through the various input-output terminals satisfy the following characteristics [Soliman, 1996]

$$i_y = 0, v_x = v_y, i_z = i_x, \text{ and } v_w = v_z, \quad (4.1)$$

where the convention for current direction is shown in Figure 4.1(a). A grounded voltage-controlled impedance gyrator was suggested by Senani et al. [2009] using CFOAs and a JFET transistor (Figure 4.1(b)). Using (4.1) the impedance of the gyrator in Figure 4.1(b) can be shown to be

$$Z_a = \frac{R_1 R_3}{Z_2 Z_4} \times r_{DS}(V_c), \quad (4.2)$$

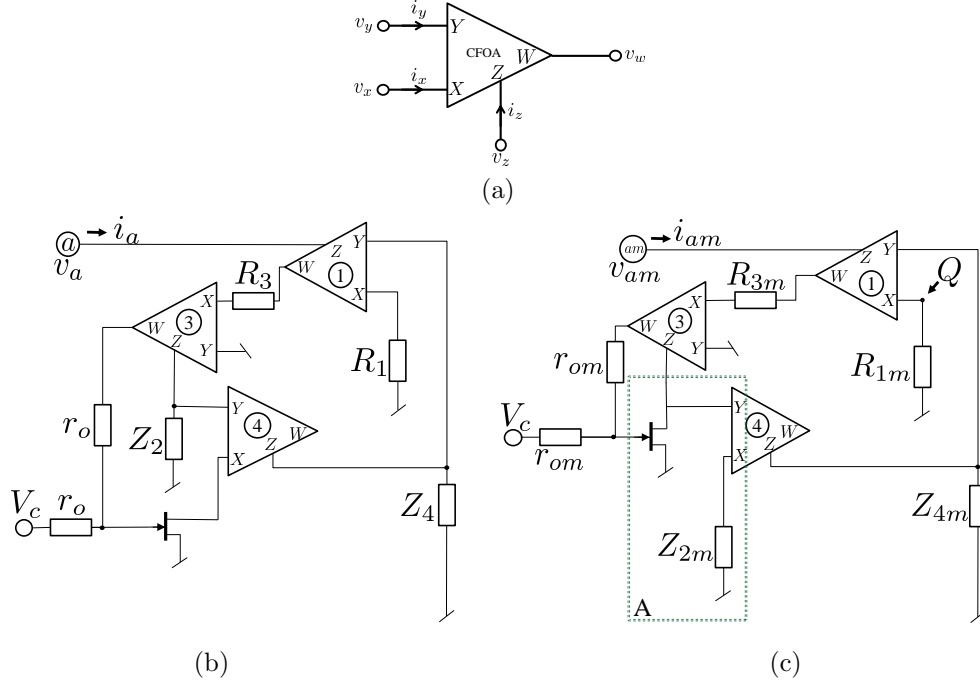


Figure 4.1: (a) Current direction convention for the CFOA, (b) grounded version of the gyrator schematic from [Senani et al., 2009], and (c) modified version with a reciprocal r_{DS} relationship to impedance.

where $r_{DS}(\cdot)$ represents the JFET drain-source resistance that is controlled by voltage, V_c , see Senani et al. [2009] for details.

In this research, we adapt from the work of Senani et al. [2009] to implement an inductor-gyrator for Chua's oscillator. To enforce $r_{DS}(\cdot)$ to have a reciprocal relationship to the total impedance, we modify the circuit of Figure 4.1(b) to that in Figure 4.1(c) which consists of swapping Z_2 and $r_{DS}(\cdot)$ with one-another. The circuit modification is explicitly highlighted in box A of Figure 4.1(c). The schematics in Figure 4.1 are drawn analogous to Senani et al. [2009] for easy comparison. As seen in the sequel, this approach will enable us to implement an adaptive parameter update law for the reciprocal of \tilde{L} in (3.4). It can be shown that the modified gyrator in Figure 4.1(c) has an impedance represented by

$$Z_{am} = \frac{R_{1m}R_{3m}Z_{2m}}{Z_{4m}} \times \frac{1}{r_{DSm}(V_c)} \quad (4.3)$$

Since the modified gyrator of Figure 4.1(c) is intended to be used as a voltage-controlled inductor, we choose R_{1m} , R_{3m} , Z_{2m} to be linear resistors ($Z_{2m} = R_{2m}$) and Z_{4m} to be a linear capacitor C ($Z_{4m} = \frac{1}{Cs}$) in the modified gyrator of Figure 4.1(c). Now the impedance of the circuit of Figure 4.1(c) can be shown to be

$$Z_{am}(s) = \frac{R_{1m}R_{2m}R_{3m}Cs}{r_{DSm}(V_c)}, \quad (4.4)$$

where s denotes the usual Laplace variable. Furthermore, we can derive the characteristic differential

equation for the circuit of Figure 4.1(c) to be

$$\frac{di_{am}}{dt} = \frac{r_{DSm}(V_c)}{R_{1m}R_{2m}R_{3m}C}v_{am}, \quad (4.5)$$

which can also be obtained by using the voltage-current relationships of (4.1) applied to the circuit of Figure 4.1(c). The current going into the modified gyrator (i_{am}) is obtained by using the voltage measured at the node Q since

$$V_Q = -i_{am}R_{1m}. \quad (4.6)$$

The modified gyrator of Figure 4.1(c) replaces the inductor \tilde{L} in Figure 2.1. Analogously a modified gyrator similar to Figure 4.1(c) replaces the inductor L in Figure 2.1 but in this case the JFET is replaced by a known fixed resistor, R_{DS} , see Figure 4.2 for further details. By applying

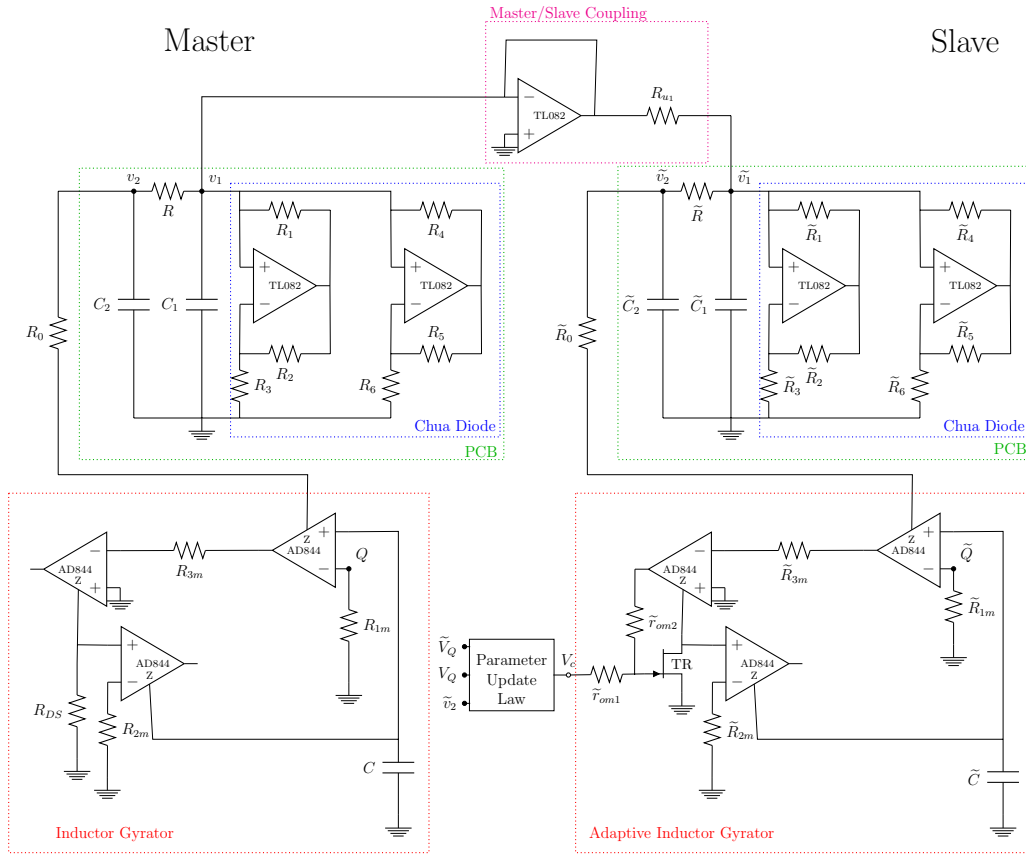


Figure 4.2: Schematic of master/slave Chua's oscillator as constructed in the experiment.

(4.4) and (4.6) for the modified gyrators used in Figure 4.2, we obtain the following

$$V_Q = i_L R_{1m}, \quad (4.7)$$

$$\tilde{V}_Q = \tilde{i}_L \tilde{R}_{1m}, \quad (4.8)$$

$$L = \frac{R_{1m} R_{2m} R_{3m} C}{R_{DS}}, \quad (4.9)$$

$$\tilde{L} = \frac{\tilde{R}_{1m} \tilde{R}_{2m} \tilde{R}_{3m} \tilde{C}}{\tilde{r}_{DSm}(V_c)}. \quad (4.10)$$

Note that, alternative voltage-controlled-parameter circuits have also been used for the Chua's oscillator for various applications [Cruz and Chua, 1993; Mayer-Kress et al., 1993; Rodriguez-Vazquez and Delgado-Restituto, 1993; Zhong et al., 1994].

Remark 4. For the physical realization of the Chua's circuit requiring adaptation of \tilde{C}_2 as in Section 3.2, a modified version the voltage-controlled capacitor-gyrator from Senani [1998] can be used.

4.2 \tilde{L} Parameter Update

The parameter update law (3.4) is implemented by using an analog multiplier, an AD633, a signal integration circuit, a reset switch, and a standard op-amp based voltage conditioning circuitry, as depicted in Figure 4.3.

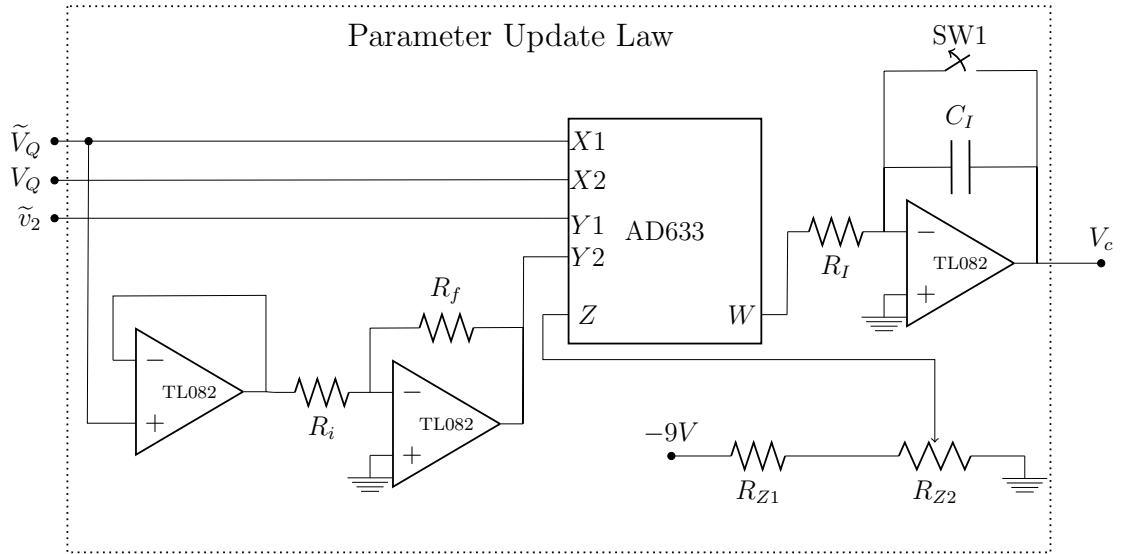


Figure 4.3: Physical realization of \tilde{L} parameter update law. R_{Z2} is tuned manually to cancel AD633 DC offset.

The AD633 has the ideal input-output relationship

$$W = \frac{(X_1 - X_2)(Y_1 - Y_2)}{10} + Z. \quad (4.11)$$

For the purposes of repeatability of our adaptive synchronization experiment, it is important to note that the intrinsic DC offset of the AD633's output W is canceled by manually tuning the potentiometer R_{Z2} . This is done prior to initiating adaptation. The integrator's initial conditions are reset to zero using the switch SW1. Knowing (4.11) and using Figure 4.3, it follows that the expression for V_c in terms of i_L , \tilde{i}_L , and \tilde{v}_2 is

$$V_c = -\frac{1}{R_I C_I} \int \left[\frac{(\tilde{R}_{1m} \tilde{i}_L - R_{1m} i_L)(\tilde{v}_2 + \tilde{i}_L \tilde{R}_{1m} \frac{R_f}{R_i})}{10} + V_{633\text{off}} + Z \right] dt, \quad (4.12)$$

where $V_{633\text{off}}$ is the DC offset of the AD633 output which is canceled with Z . Note that in our experiments $V_{633\text{off}}$ is found to be positive. If $V_{633\text{off}}$ happens to be negative, the supply voltage for voltage divider producing Z can be made +9V. In an ideal case, we can assume that

$$\tilde{R}_{1m} = R_{1m}, \quad (4.13)$$

$$Z = -V_{633\text{off}}, \quad (4.14)$$

$$\tilde{R}_{1m} \frac{R_f}{R_i} = R_0, \quad (4.15)$$

$$\tilde{r}_{DSm} = -aV_c + c, \quad \text{where } a > 0 \text{ and } c > 0. \quad (4.16)$$

Equation (4.16) is an approximation from the empirical results of Nay and Budak [1983].

By inverting (4.10), substituting for \tilde{r}_{DSm} using (4.16), and using (4.12)–(4.15), we obtain the following

$$\frac{1}{\tilde{L}} = \frac{a}{\tilde{R}_{2m} \tilde{R}_{3m} \tilde{C}} \times \frac{1}{10 R_I C_I} \int e_{i_L} (\tilde{v}_2 + \tilde{i}_L R_0) dt + \frac{c}{\tilde{R}_{1m} \tilde{R}_{2m} \tilde{R}_{3m} \tilde{C}}. \quad (4.17)$$

Next, taking the derivative of (4.17) with respect to time yields

$$\frac{d}{dt} \left(\frac{1}{\tilde{L}} \right) = \frac{a}{10 \tilde{R}_{2m} \tilde{R}_{3m} \tilde{C} R_I C_I} e_{i_L} (\tilde{v}_2 + \tilde{i}_L R_0), \quad (4.18)$$

confirming that the schematic in Figure 4.3 implements the parameter update law (3.4) and that

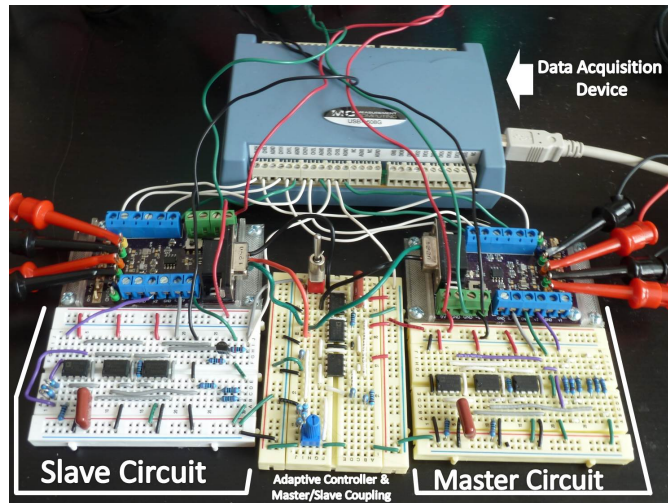
$$\gamma = \frac{a}{10 \tilde{R}_{2m} \tilde{R}_{3m} \tilde{C} R_I C_I}. \quad (4.19)$$

4.3 Experimental Setup

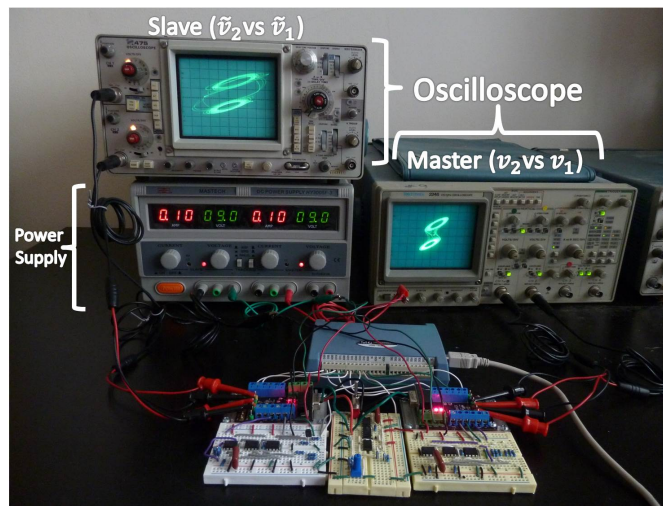
Figures 4.2 and 4.3 contain the complete circuit schematics that are used in the physical implementation of master/slave Chua’s oscillator synchronization with adaptive parameter update law for \tilde{L} . The parts of the circuit constructed using two identical, dual layer printed circuit boards (PCBs), which utilize surface-mount technology (SMT) components, are highlighted in Figure 4.2. The remaining circuitry is built using solderless breadboards with through-hole (THL) components. The custom PCBs of the master/slave system are connected to a data acquisition device, two analog oscilloscopes, and a regulated $\pm 9V$ power supply. Specifically, we used Measurement Computing’s USB-1608G data acquisition device, which is sampled at 62.5 kHz to collect the experimental data. Since USB-1608G can simultaneously sample only four signals at 62.5 kHz, we run each experiment twice. In the first experimental run, we use USB-1608G in differential mode to acquire $\tilde{V}_Q - V_Q$, $\tilde{v}_2 - v_2$, $\tilde{v}_1 - v_1$, and $V_c - \text{GND}$ to examine synchronization between the master/slave system. In the second experimental run, we use USB-1608G to acquire v_2 , V_Q , \tilde{v}_2 , \tilde{V}_Q signals for parameter estimation. Photographic images of the experimental setup are shown in Figure 4.4. To test this setup for different parameter values of the master/slave system, we can simply vary the resistances (e.g., $R_{im}, i = 1, 2, 3$) on the solderless breadboards. The components that remain constant for all cases are listed in Table 4.1. Note that, we use the shorthand notation $||$ and $+$ for components connected in parallel and series, respectively. When appropriate, the setup is placed inside a grounded metal housing to eliminate electromagnetic interference (EMI).

Table 4.1: Constant Components

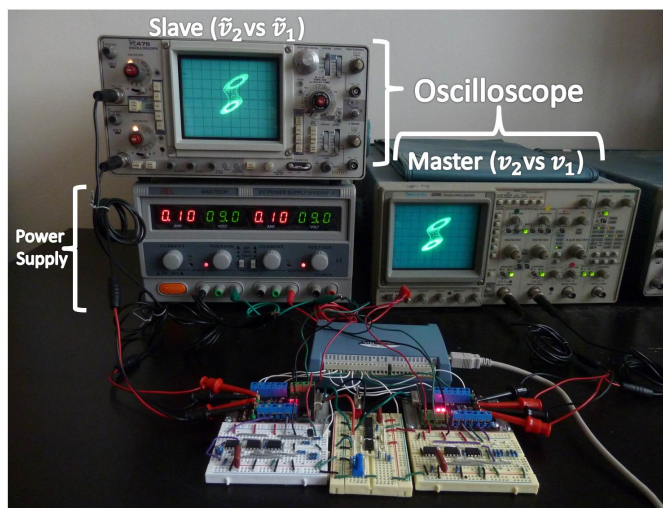
Master Chua's Oscillator	Adaptive Controller	Slave Chua's Oscillator
$R_1 = 22 \text{ k}\Omega$ 0.1% SMT $R_2 = 22 \text{ k}\Omega$ 0.1% SMT $R_3 = 3.3 \text{ k}\Omega$ 0.1% SMT $R_4 = 220 \Omega$ 0.1% SMT $R_5 = 220 \Omega$ 0.1% SMT $R_6 = 2.2 \text{ k}\Omega$ 0.1% SMT $R = 3.4 \text{ k}\Omega \parallel 3.4 \text{ k}\Omega$ (0.1% each) SMT $C_1 = 10 \text{ nF}$ 1% SMT $C_2 = 100 \text{ nF}$ 1% SMT $C = 18 \text{ nF}$ 3% THL $R_{1m} = 1 \text{ k}\Omega$ 0.1% THL $R_{3m} = 1 \text{ k}\Omega$ 0.1% THL $R_{DS} = 1 \text{ k}\Omega$ 0.1% THL	$R_{u1} = 500 \Omega$ 1% THL $R_f = 1 \text{ k}\Omega$ 0.1% THL $C_f = 18 \text{ nF}$ 3% THL $R_{Z1} = 200 \text{ k}\Omega + 200 \text{ k}\Omega + 200 \text{ k}\Omega$ $+ 200 \text{ k}\Omega$ (1% each) THL $R_{Z2} = 1 \text{ k}\Omega$ pot THL	$\tilde{R}_1 = 22 \text{ k}\Omega$ 0.1% SMT $\tilde{R}_2 = 22 \text{ k}\Omega$ 0.1% SMT $\tilde{R}_3 = 3.3 \text{ k}\Omega$ 0.1% SMT $\tilde{R}_4 = 220 \Omega$ 0.1% SMT $\tilde{R}_5 = 220 \Omega$ 0.1% SMT $\tilde{R}_6 = 2.2 \text{ k}\Omega$ 0.1% SMT $\tilde{R} = 3.4 \text{ k}\Omega \parallel 3.4 \text{ k}\Omega$ (0.1% each) SMT $\tilde{C}_1 = 10 \text{ nF}$ 1% SMT $\tilde{C}_2 = 100 \text{ nF}$ 1% SMT $\tilde{C} = 18 \text{ nF}$ 3% THL $\tilde{R}_{1m} = 1 \text{ k}\Omega$ 0.1% THL $\tilde{R}_{3m} = 1 \text{ k}\Omega$ 0.1% THL $\text{TR} = 2\text{N}3819$ THL $\tilde{r}_{om1} = 10 \text{ k}\Omega$ 1% THL $\tilde{r}_{om2} = 10 \text{ k}\Omega$ 1% THL



(a)



(b)



(c)

Figure 4.4: Experimental setup: (a) close up of circuitry and data acquisition device, (b) full setup when switch SW1 is closed, and (c) full setup when switch SW1 is open.

Chapter 5

Experimental, SPICE, and MATLAB Results

5.1 Experimental Results

This research is concerned with an experimental implementation of adaptive parameter tuning in the context of synchronization of analog Chua’s oscillators. To illustrate our ability to tune parameter \tilde{L} to match L , we provide results from four experiments, each using a different value of L . To change L , we only modify R_{2m} according to (4.9). Experiments 1–3 are designed to demonstrate the performance of the adaptive controller when the Chua’s oscillator is chaotic. As the value of L is changed in each experiment, to ensure that the resulting circuit remains chaotic, we must also change R_0 . Thus, following (4.15), any change in R_0 also necessitates corresponding changes in R_i and R_f . Moreover, for the slave Chua’s oscillator, we select \tilde{R}_{2m} and \tilde{R}_0 resistor values to be same as the ones for the master Chua’s oscillator, i.e., $\tilde{R}_{2m} = R_{2m}$ and $\tilde{R}_0 = R_0$. Experiment 4 is performed to demonstrate the performance of the adaptive controller when the Chua’s oscillator is periodic, hence only R_{2m} and \tilde{R}_{2m} are changed. The resistor components selected for Experiments 1–4 are listed in Tables 5.1–5.4, respectively.

To quantify how well the master/slave system synchronizes, we use the 2-norm of $[e_{i_L}, e_{v_2}, e_{v_1}]^T$ as our measure, ($e_{\text{norm}} \triangleq \|[e_{i_L} e_{v_2} e_{v_1}]^T\|$), and observe its evolution over time. Using the signals \tilde{i}_L and \tilde{v}_2 we estimate \tilde{L} and \tilde{R}_0 ($\tilde{L}_{\text{est}}, \tilde{R}_{0\text{est}}$) with a sliding window least square algorithm. Similarly, using signals i_L and v_2 we estimate L and R_0 ($L_{\text{est}}, R_{0\text{est}}$). Comparing these estimates allows us to examine how well \tilde{L} converges to L . The transient experimental data of Experiments 1–4 is displayed in Figures 5.1–5.4, respectively, each divided into parts (a)–(e). The vertical bars in Figures 5.1(b)–5.4(b) indicate when SW1 is opened so that V_c switches from a zero value to a non-zero value, which can be used to indicate the initiation of adaptation. No vertical bar is seen in Figures 5.1(c)–5.4(c) because in this case V_c is not being measured explicitly and thus we are unable to pin-point the exact instance when SW1 is opened for the second experimental run.

Note that, each point on Figures 5.1(c)–5.4(c) represents a least square estimate of a window of 50 samples and the x -axis indicates the time when the leading sample is taken. Figures 5.1(d)–5.4(d) and Figures 5.1(e)–5.4(e) re-plot the last 10 ms of Figures 5.1(b)–5.4(b) and Figures 5.1(c)–5.4(c), respectively, to better visualize the steady-state results. The average of each signal (except V_c) in sections (d) and (e) is listed in Tables 5.1–5.4.

Table 5.1: Experiment 1

$R_{2m} = 2.2 \text{ k}\Omega + (100 \text{ }\Omega \parallel 100 \text{ }\Omega) \text{ (0.1 \% each) THL}$	$L = 40.5 \text{ mH}$ according to (4.9)
$\tilde{R}_{2m} = 2.2 \text{ k}\Omega + (100 \text{ }\Omega \parallel 100 \text{ }\Omega) \text{ (0.1 \% each) THL}$	$L_{\text{est}} = 50.8 \text{ mH}$ (average)
$R_i = 2.2 \text{ k}\Omega \parallel 2.2 \text{ k}\Omega \text{ (0.1 \% each) THL}$	$\tilde{L}_{\text{est}} = 51.8 \text{ mH}$ (average)
$R_f = 220 \text{ }\Omega \text{ (0.1 \% each) THL}$	$e_{\text{norm}} = 1.57 \times 10^{-2}$ (average)
$R_0 = 100 \text{ }\Omega + 100 \text{ }\Omega \text{ (0.1 \% each) THL} \approx 200 \text{ }\Omega$	$R_{0\text{est}} = 225.54 \text{ }\Omega$ (average)
$\tilde{R}_0 = 100 \text{ }\Omega + 100 \text{ }\Omega \text{ (0.1 \% each) THL} \approx 200 \text{ }\Omega$	$\tilde{R}_{0\text{est}} = 225.64 \text{ }\Omega$ (average)

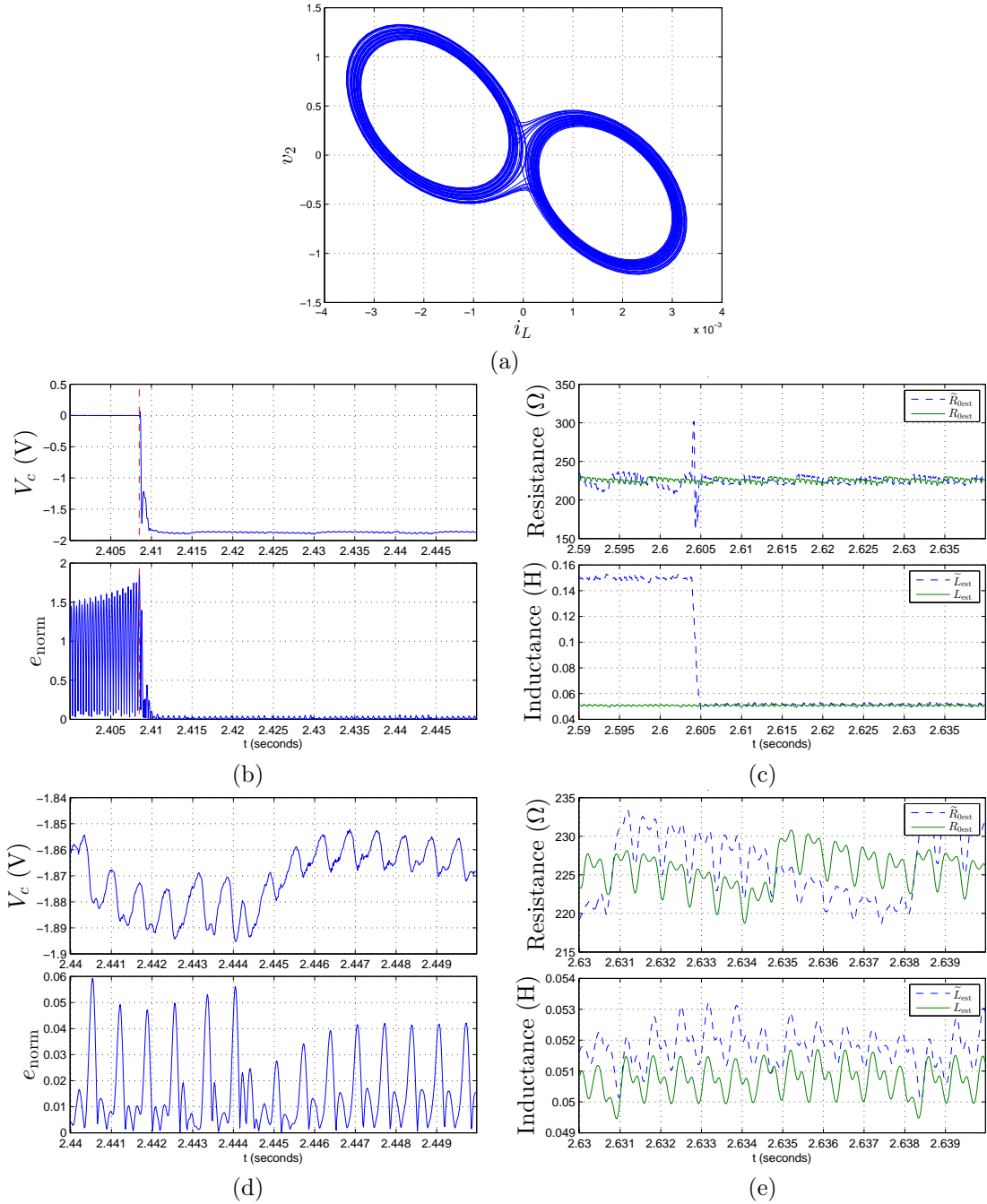


Figure 5.1: Experiment 1

Table 5.2: Experiment 2

$R_{2m} = 1 \text{ k}\Omega + 1 \text{ k}\Omega$ (0.1 % each) THL $\tilde{R}_{2m} = 1 \text{ k}\Omega + 1 \text{ k}\Omega$ (0.1 % each) THL $R_i = 1 \text{ k}\Omega \parallel 2.2 \text{ k}\Omega$ (0.1 % each) THL $R_f = 220 \text{ }\Omega + 220 \text{ }\Omega$ (0.1 % each) THL $R_0 = (220 \text{ }\Omega \parallel 220 \text{ }\Omega) + (100 \text{ }\Omega \parallel 100 \text{ }\Omega)$ (0.1 % each) THL $\approx 160 \text{ }\Omega$ $\tilde{R}_0 = (220 \text{ }\Omega \parallel 220 \text{ }\Omega) + (100 \text{ }\Omega \parallel 100 \text{ }\Omega)$ (0.1 % each) THL $\approx 160 \text{ }\Omega$	$L = 36.0 \text{ mH}$ according to (4.9) $L_{\text{est}} = 45.2 \text{ mH}$ (average) $\tilde{L}_{\text{est}} = 46.3 \text{ mH}$ (average) $e_{\text{norm}} = 1.51 \times 10^{-2}$ (average) $R_{0\text{est}} = 186.23 \text{ }\Omega$ (average) $\tilde{R}_{0\text{est}} = 186.06 \text{ }\Omega$ (average)
--	---

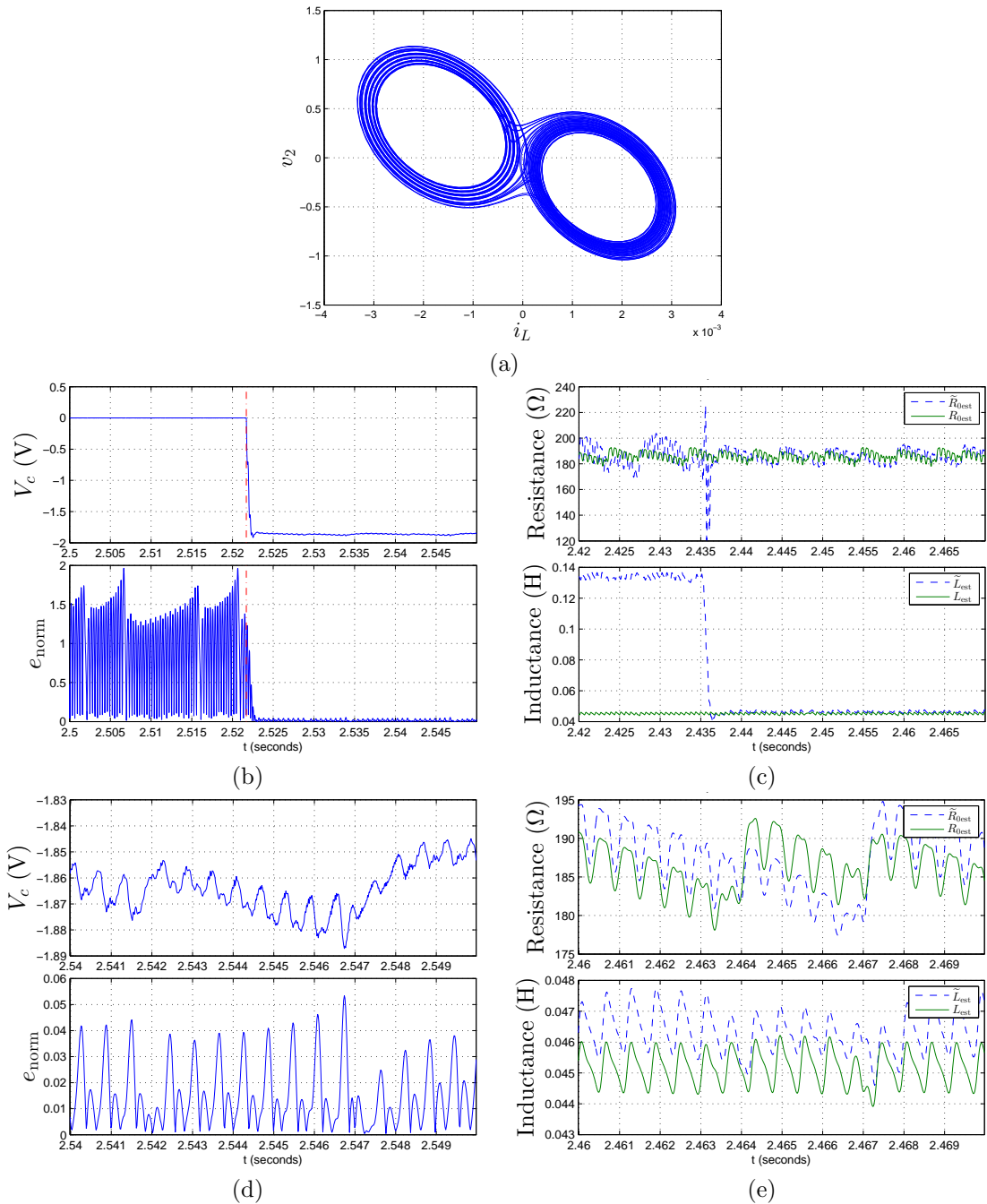


Figure 5.2: Experiment 2

Table 5.3: Experiment 3

$R_{2m} = 1 \text{ k}\Omega + (1 \text{ k}\Omega \parallel 1 \text{ k}\Omega)$ (0.1 % each) THL	$L = 27.0 \text{ mH}$ according to (4.9)
$\tilde{R}_{2m} = 1 \text{ k}\Omega + (1 \text{ k}\Omega \parallel 1 \text{ k}\Omega)$ (0.1 % each) THL	$L_{\text{est}} = 34.1 \text{ mH}$ (average)
$R_i = 1 \text{ k}\Omega + 100 \text{ }\Omega + 100 \text{ }\Omega$ (0.1 % each) THL	$\tilde{L}_{\text{est}} = 32.8 \text{ mH}$ (average)
$R_f = 100 \text{ }\Omega$ (0.1 %) THL	$e_{\text{norm}} = 1.49 \times 10^{-2}$ (average)
$R_0 = 1 \text{ k}\Omega \parallel 1 \text{ k}\Omega \parallel 100 \text{ }\Omega$ (0.1 % each) THL $\approx 83.333 \text{ }\Omega$	$R_{0\text{est}} = 114.33 \text{ }\Omega$ (average)
$\tilde{R}_0 = 1 \text{ k}\Omega \parallel 1 \text{ k}\Omega \parallel 100 \text{ }\Omega$ (0.1 % each) THL $\approx 83.333 \text{ }\Omega$	$\tilde{R}_{0\text{est}} = 117.35 \text{ }\Omega$ (average)

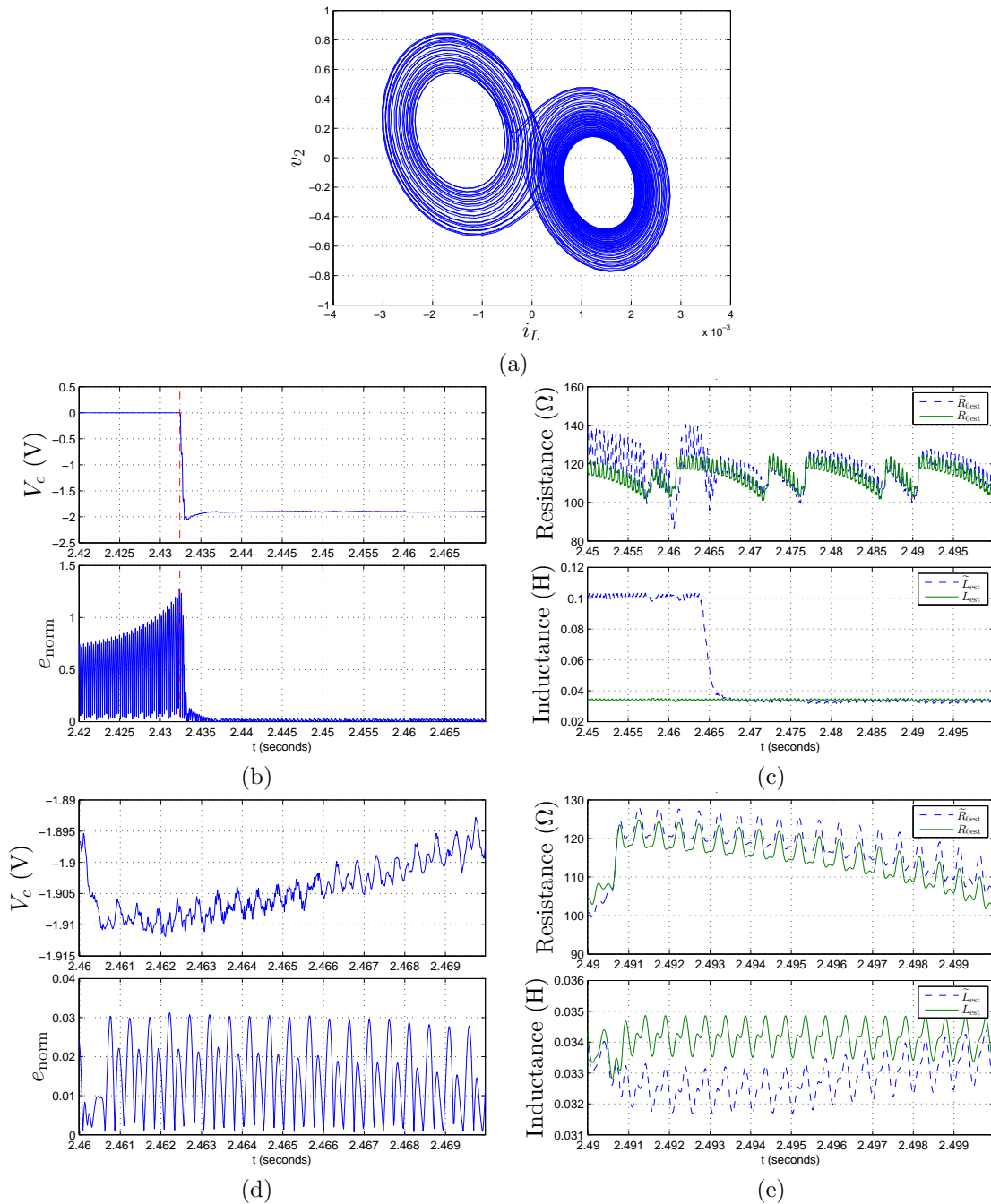


Figure 5.3: Experiment 3

Table 5.4: Experiment 4

$R_{2m} = (1 \text{ k}\Omega + 3.3 \text{ k}\Omega) \parallel 2.2 \text{ k}\Omega$ (0.1 % each) THL	$L = 26.2 \text{ mH}$ according to (4.9)
$\tilde{R}_{2m} = (1 \text{ k}\Omega + 3.3 \text{ k}\Omega) \parallel 2.2 \text{ k}\Omega$ (0.1 % each) THL	$L_{\text{est}} = 33.1 \text{ mH}$ (average)
$R_i = 1 \text{ k}\Omega + 100 \Omega + 100 \Omega$ (0.1 % each) THL	$\tilde{L}_{\text{est}} = 32.5 \text{ mH}$ (average)
$R_f = 100 \Omega$ (0.1 %) THL	$e_{\text{norm}} = 1.11 \times 10^{-2}$ (average)
$R_0 = 1 \text{ k}\Omega \parallel 1 \text{ k}\Omega \parallel 100 \Omega$ (0.1 % each) THL $\approx 83.333 \Omega$	$R_{0\text{est}} = 103.53 \Omega$ (average)
$\tilde{R}_0 = 1 \text{ k}\Omega \parallel 1 \text{ k}\Omega \parallel 100 \Omega$ (0.1 % each) THL $\approx 83.333 \Omega$	$\tilde{R}_{0\text{est}} = 107.30 \Omega$ (average)

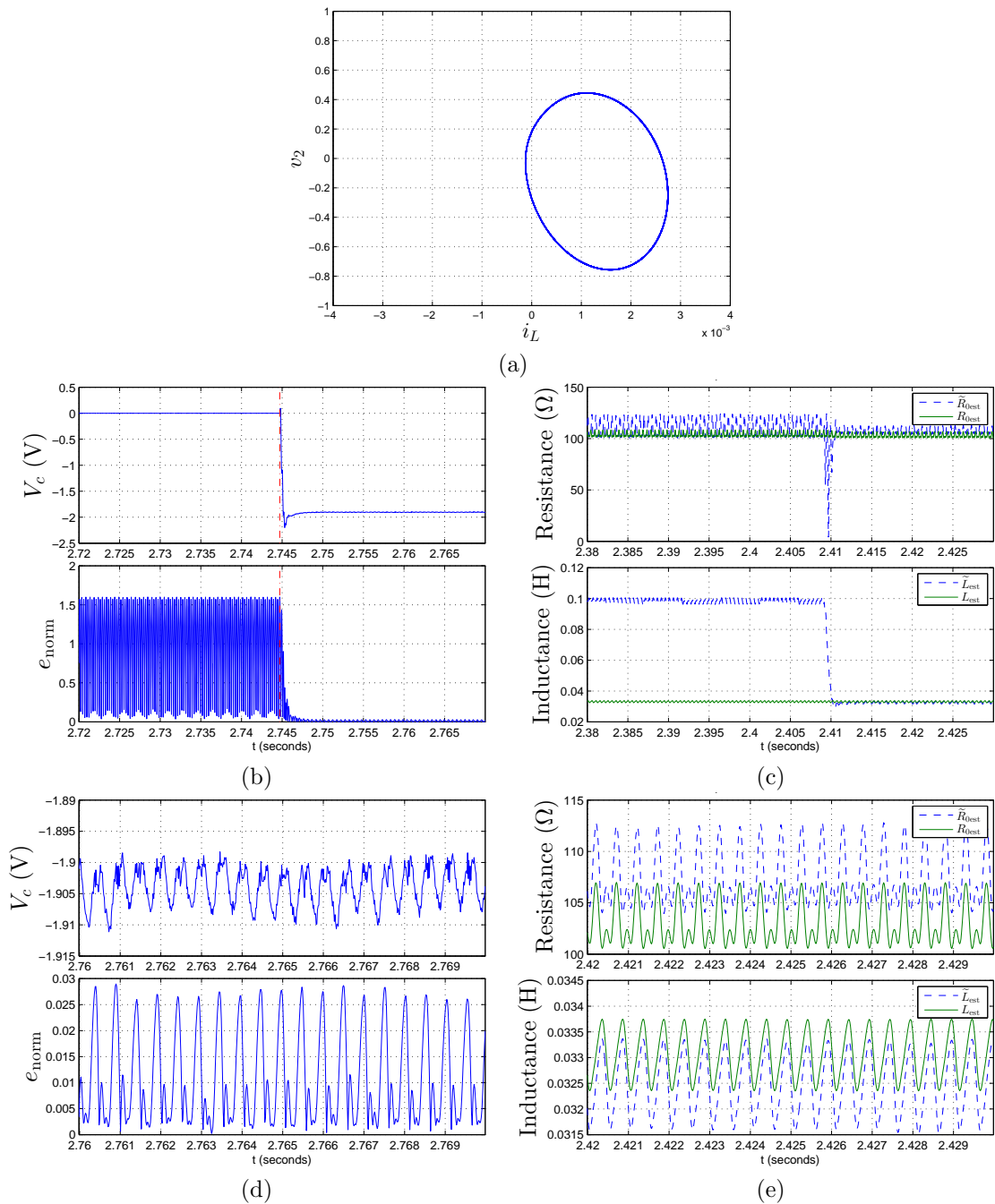


Figure 5.4: Experiment 4

5.2 SPICE Simulation Results

SPICE simulations of the experiment are done to compare with experimental results and to examine the influence of noise and unmodeled parasitic effects on the experimental results. Hence, we develop a SPICE simulation model containing the various non-ideal behaviors of components such that the simulation model closely replicates the experimental system (see Figure A.1). This includes extracting the signals i_L and \tilde{i}_L by measuring the voltages at nodes Q and \tilde{Q} in the SPICE simulation as opposed to directly extracting the i_L and \tilde{i}_L . The SPICE simulator TINA-TI V9 [TexasInstruments, 2008] is chosen because of the capability of its numerical solver to optimize its tolerance parameters for convergence. As shown in Figure 4.2, the physical experiment uses three distinct integrated circuits (ICs), the AD844, the AD633, and the TL082. High fidelity SPICE Macro-Models [AnalogDevices, 2013a,b; TexasInstruments, 2013] of each IC are used in the SPICE simulations. Similarly, the JFET used in the experiment, the 2N3819, is modeled in TINA-TI V9 using the Schickman-Hodges model with specific parameters for the 2N3819 already embedded in the software. Simulations are run using the order 2 trapezoidal integration method. SPICE Simulations 1 and 2 have different initial conditions and adaptive parameter update initiation times from SPICE Simulations 3 and 4. SPICE Simulations 1 and 2 initial conditions are set to -0.6 V and 0.6 V for v_2 and \tilde{v}_2 , respectively, with an adaptive parameter update initiation time starting at 25 ms. SPICE Simulations 3 and 4 initial conditions are set to -9 V and 9 V for v_2 and \tilde{v}_2 , respectively, with an adaptive parameter update initiation time starting at 60ms. Different initial conditions and times to switch SW1 are selected to replicate orbits from the experiment and the time it takes to reach those orbits. Since the AD633 Z input is tuned manually in the experiment, the distinct differences between the schematic in Figure 4.2 and the SPICE model is that the AD633 input terminal Z has a direct -5 mV source connected to it as opposed to the wiper of the potentiometer R_{Z2} as in Figure 4.2.

Two types of simulations are performed. The first type of simulations use the ideal values of the passive components of Experiments 1 and 4 (SPICE Simulations 1 and 3). The second type of simulations use the ideal values of the passive components of Experiments 1 and 4 for the master Chua's oscillator and numerical values of passive components in the slave Chua's oscillator and adaptive controller are increased by their respective tolerances (SPICE Simulations 2 and 4). Note that, in SPICE Simulations 3 and 4, to replicate the same periodic behavior as in Experiment 4, the ideal values of R_{2m} and \tilde{R}_{2m} are changed to 1.3 k Ω . Results are displayed similar to Section 4.3 in Tables 5.5–5.8 and Figures 5.5–5.8.

Table 5.5: SPICE Simulation 1

$R_{2m} = 2.25 \text{ k}\Omega$	$L = 40.5 \text{ mH}$ according to (4.9)
$\tilde{R}_{2m} = 2.25 \text{ k}\Omega$	$L_{\text{est}} = 45.4 \text{ mH}$ (average)
$R_i = 1.1 \text{ k}\Omega$	$\tilde{L}_{\text{est}} = 45.4 \text{ mH}$ (average)
$R_f = 220 \text{ }\Omega$	$e_{\text{norm}} = 1.6 \times 10^{-3}$ (average)
$R_0 = 200 \text{ }\Omega$	$R_{0\text{est}} = 202.42 \text{ }\Omega$ (average)
$\tilde{R}_0 = 200 \text{ }\Omega$	$\tilde{R}_{0\text{est}} = 202.46 \text{ }\Omega$ (average)

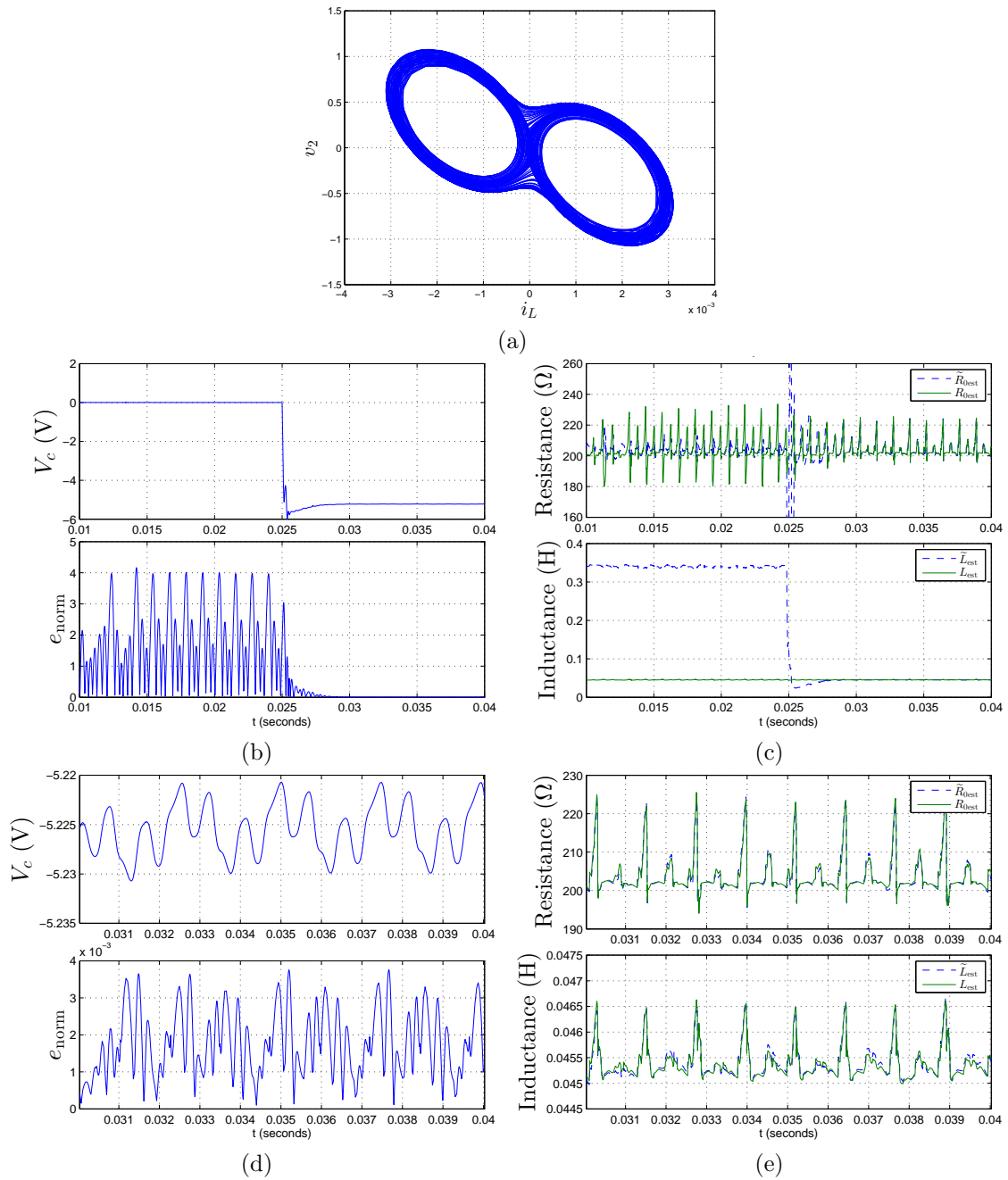


Figure 5.5: SPICE Simulation 1

Table 5.6: SPICE Simulation 2

$R_{2m} = 2.25 \text{ k}\Omega$	$L = 40.5 \text{ mH}$ according to (4.9)
$\tilde{R}_{2m} = 2.25225 \text{ k}\Omega$	$L_{\text{est}} = 45.4 \text{ mH}$ (average)
$R_i = 1.1011 \text{ k}\Omega$	$\tilde{L}_{\text{est}} = 45.3 \text{ mH}$ (average)
$R_f = 220.22 \text{ }\Omega$	$e_{\text{norm}} = 1.8 \times 10^{-3}$ (average)
$R_0 = 200 \text{ }\Omega$	$R_{0\text{est}} = 202.89 \text{ }\Omega$ (average)
$\tilde{R}_0 = 200.2 \text{ }\Omega$	$\tilde{R}_{0\text{est}} = 202.84 \text{ }\Omega$ (average)

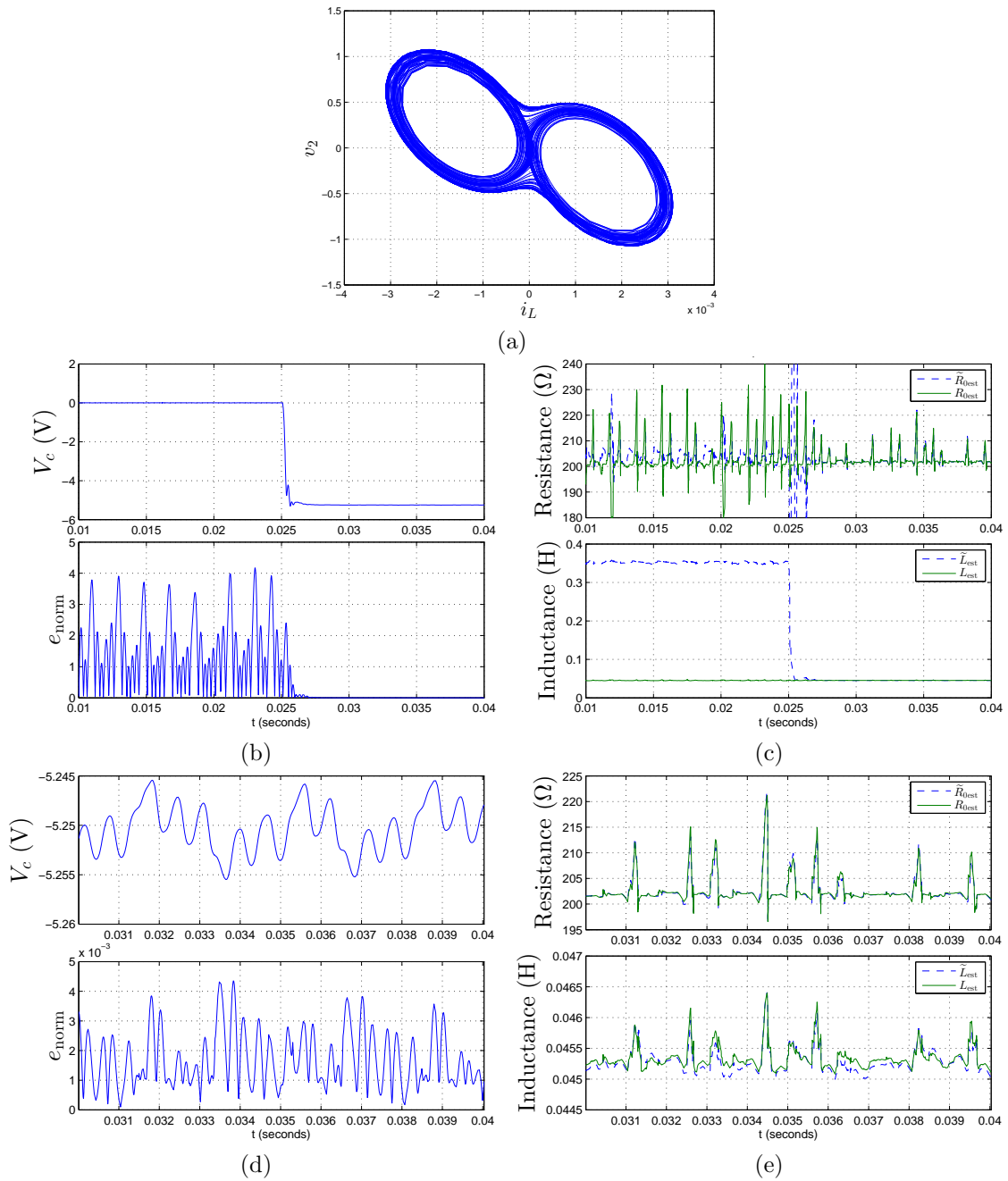


Figure 5.6: SPICE Simulation 2

Table 5.7: SPICE Simulation 3

$R_{2m} = 1.3 \text{ k}\Omega$	$L = 23.4 \text{ mH}$ according to (4.9)
$\tilde{R}_{2m} = 1.3 \text{ k}\Omega$	$L_{\text{est}} = 26.8 \text{ mH}$ (average)
$R_i = 1.2 \text{ k}\Omega$	$\tilde{L}_{\text{est}} = 26.8 \text{ mH}$ (average)
$R_f = 100 \text{ }\Omega$	$e_{\text{norm}} = 10^{-3}$ (average)
$R_0 = 83.33 \text{ }\Omega$	$R_{0\text{est}} = 85.78 \text{ }\Omega$ (average)
$\tilde{R}_0 = 83.33 \text{ }\Omega$	$\tilde{R}_{0\text{est}} = 85.92 \text{ }\Omega$ (average)

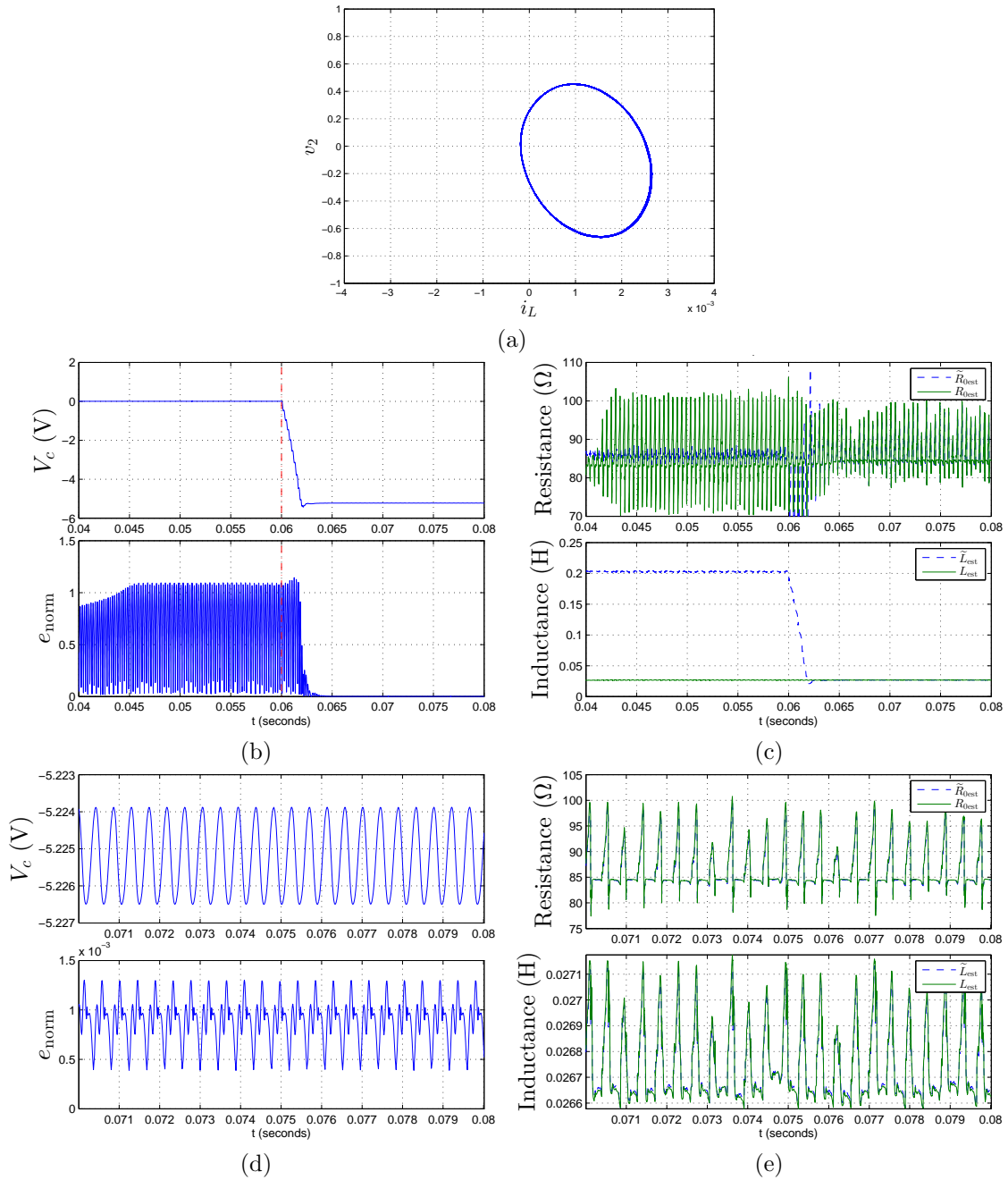


Figure 5.7: SPICE Simulation 3

Table 5.8: SPICE Simulation 4

$R_{2m} = 1.3 \text{ k}\Omega$	$L = 23.4 \text{ mH}$ according to (4.9)
$\tilde{R}_{2m} = 1.3013 \text{ k}\Omega$	$L_{\text{est}} = 26.8 \text{ mH}$ (average)
$R_i = 1.2012 \text{ k}\Omega$	$\tilde{L}_{\text{est}} = 26.7 \text{ mH}$ (average)
$R_f = 100.1 \text{ }\Omega$	$e_{\text{norm}} = 9.72 \times 10^{-4}$ (average)
$R_0 = 83.33 \text{ }\Omega$	$R_{0\text{est}} = 85.82 \text{ }\Omega$ (average)
$\tilde{R}_0 = 83.4167 \text{ }\Omega$	$\tilde{R}_{0\text{est}} = 85.60 \text{ }\Omega$ (average)

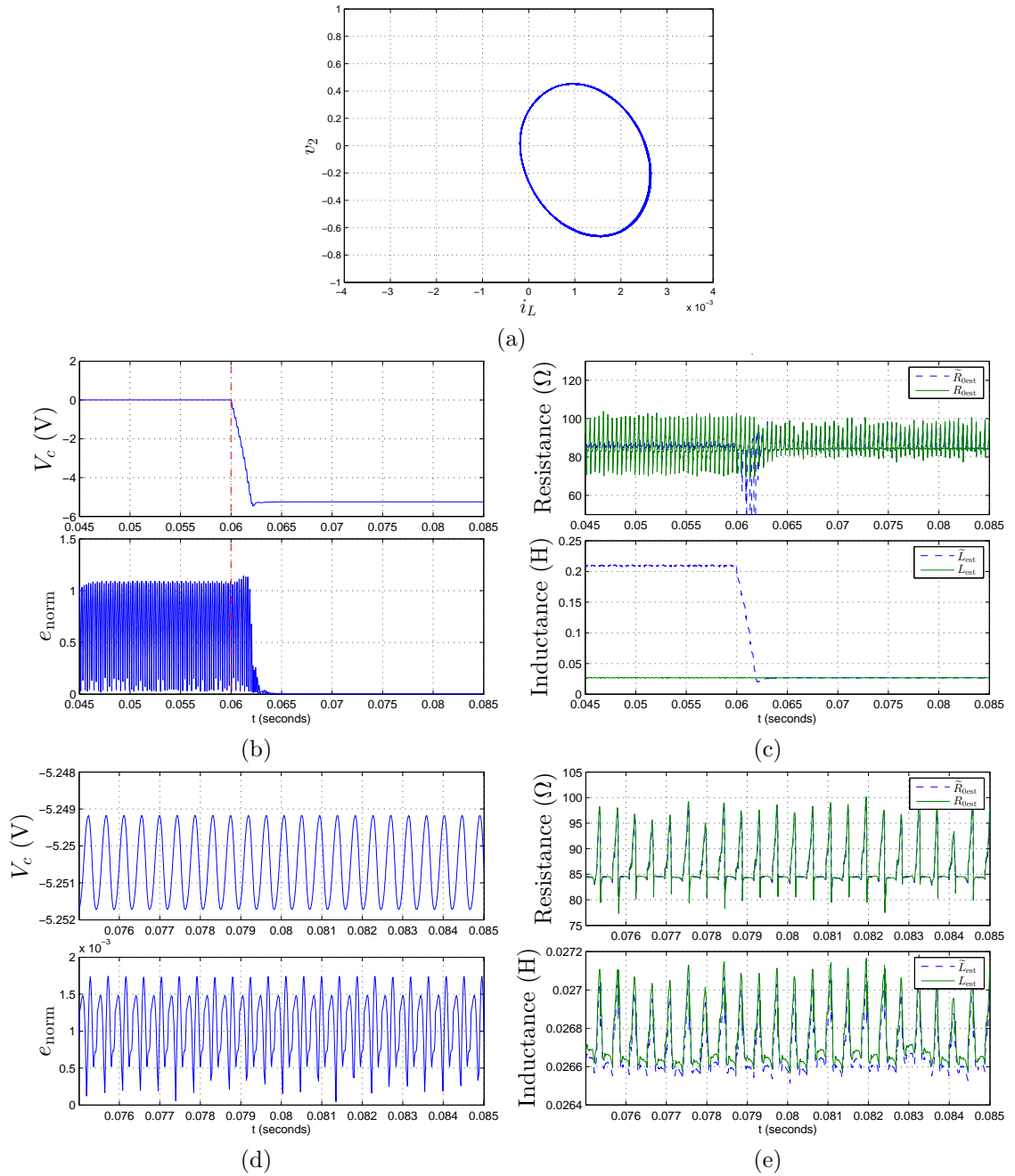


Figure 5.8: SPICE Simulation 4

5.3 MATLAB Simulation Results

Four sets of MATLAB-Simulink simulations are run to map the performance of the adaptive control laws derived in Sections 3.1 and 3.2 as a function of the behavior of the master Chua's oscillator which changes from chaotic to equilibrium behavior. Each set of simulations is run 1,000 times for 1,000 different values of C_1 ranging from 10 nF to 13 nF. With each change in the C_1 value, the simulation result for the master Chua's attractor also changes. Details of the MATLAB-Simulink simulations are described in Appendix B. To illustrate the change in the master Chua's attractor with the change in the value of C_1 , Figure 5.9 provides the bifurcation diagram for the master Chua's oscillator for the 1,000 values of C_1 . The first two sets of simulations, namely, MATLAB Simulations 1 and 2, implement the adaptive control laws of Section 3.1 and 3.2, respectively. To capture the impact of component tolerances, the next two sets of simulations, namely, MATLAB Simulations 3 and 4, implement the adaptive control laws of Section 3.1 and 3.2, respectively, with the slave Chua's oscillator parameters increased by 0.1% (not including C_1).

The common setup for all simulations is as follows: simulations are run by using the Runge-Kutta 4th order numerical solver with a fixed step-size of 10 microseconds for a simulation time of two seconds. The initial conditions are selected to be $v_1(0) = 1$, $v_2(0) = 0$, $i_L(0) = 0$, $\tilde{v}_1(0) = 2$, $\tilde{v}_2(0) = 0$, and $\tilde{i}_L(0) = 0$. Since it takes time for the master Chua's oscillator to evolve from the initial condition to reach the attractor corresponding to the chosen C_1 value, the parameter update law is activated only after 0.5 seconds into the simulation. The parameters used in simulations are listed in Table 5.9. Figure 5.10–5.13 show the simulation results for MATLAB Simulations 1–4. Figures 5.10–5.11 use three measures to examine the performance of the adaptive controller. The first performance measure is the error $e_\rho(t = 2)$ and $e_\pi(t = 2)$, that is the parameter error after two seconds of simulation time. The second performance measure is $e_{\text{norm}}(t = 2)$, that is the norm of the error state vector after two seconds of simulation time. Finally, the third performance measure is the settling time (t_{st}), that is the time it takes the slave oscillator's adaptive parameter to reach within 10% of the master's corresponding fixed parameter. Figure 5.12–5.13 use the same measures except e_ρ , e_π , and e_{norm} are averaged over the last 10 ms of simulation time. Unlike the ideal simulations (MATLAB Simulations 1 and 2) which converge exponentially, MATLAB Simulations 3 and 4 behave as in Parlitz and Kocarev [1996] where the adaptive parameter oscillates around a value slightly offset from the ideal.

Table 5.9: MATLAB Simulation Parameters

Common Parameters	MATLAB Simulations 1 and 3	MATLAB Simulations 2 and 4
$G = \tilde{G} = 1/1700 \text{ S}$	$\gamma = 5 \times 10^7$	$\eta = 10^{13}$
$R_0 = \tilde{R}_0 = 13 \text{ } \Omega$	$C_2 = \tilde{C}_2 = 100 \text{ nF}$	$L = \tilde{L} = 18 \text{ mH}$
$G_a = -0.40909 \text{ mS}$	$L = 18 \text{ mH}$	$C_2 = 100 \text{ nF}$
$G_b = -0.75758 \text{ mS}$	$\tilde{L}(0) = 10 \text{ mH}$	$\tilde{C}_2(0) = 80 \text{ nF}$
$E_1 = 1.1739 \text{ V}$		
$G_{u_1} = 1/500 \text{ S}$		

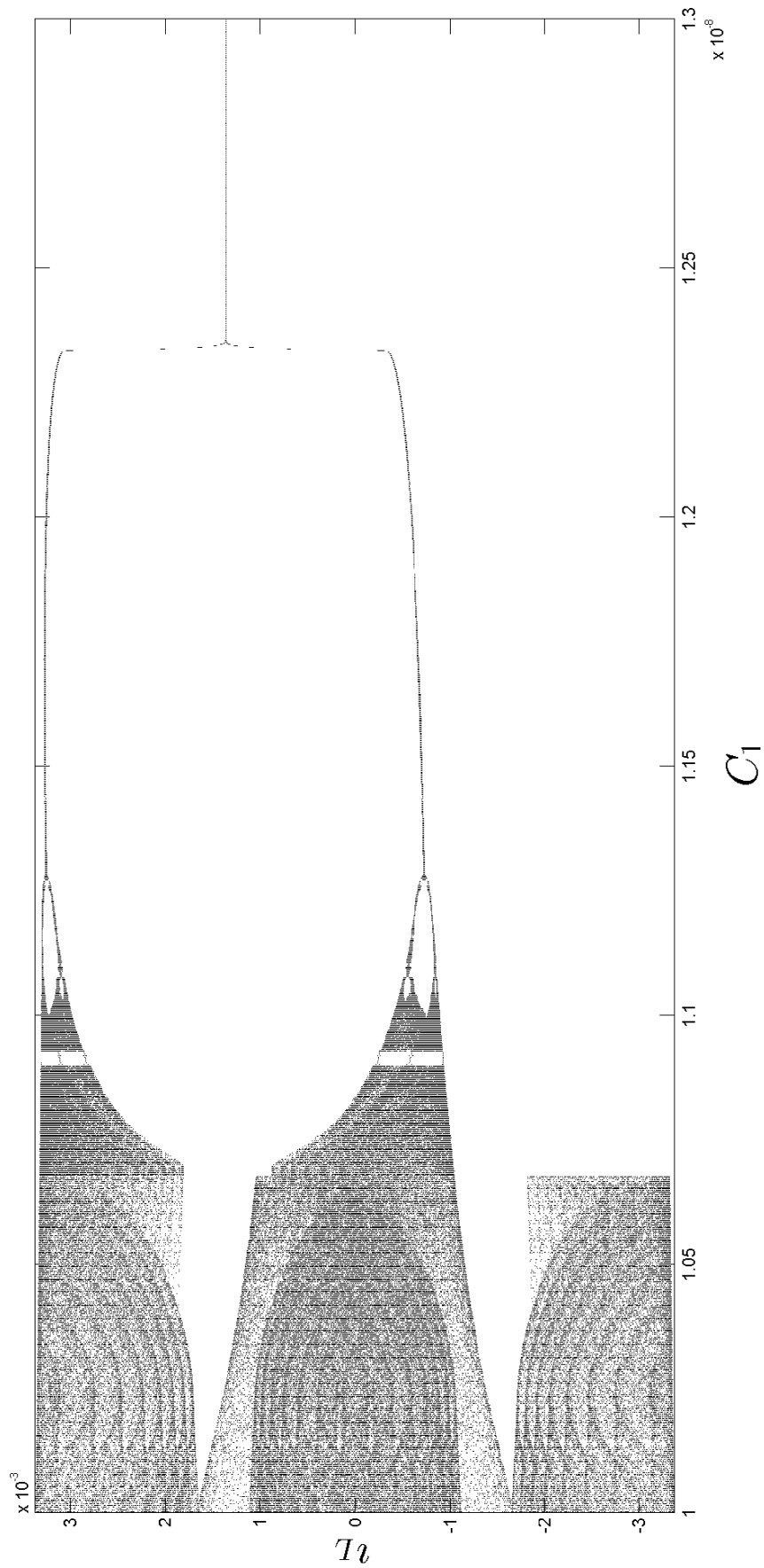


Figure 5.9: Chua's oscillator bifurcation diagram along C_1 .

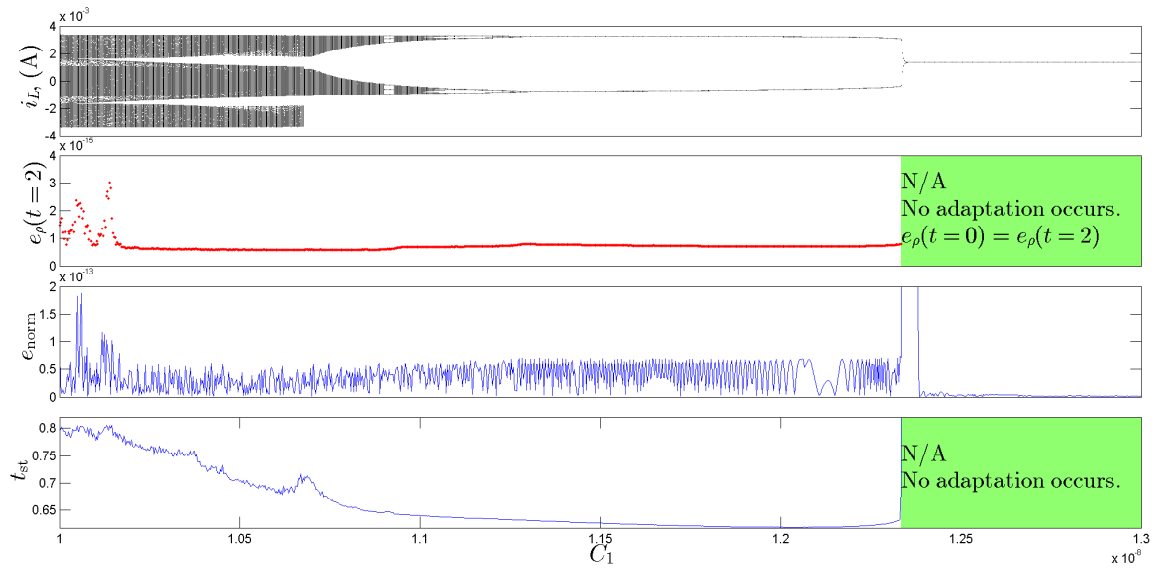


Figure 5.10: MATLAB Simulation 1: Adapting for \tilde{L}

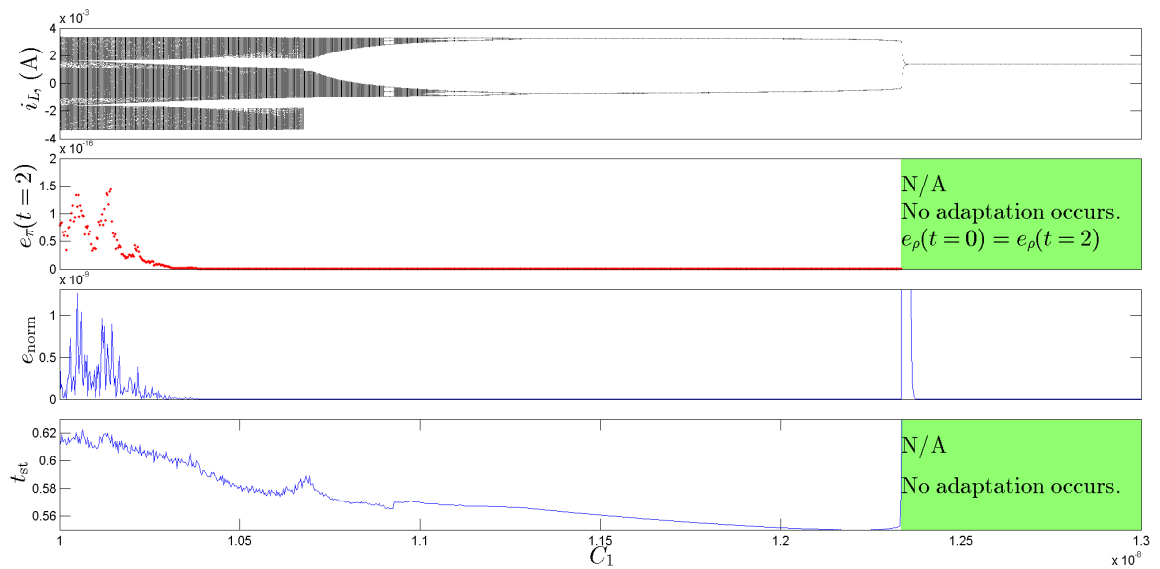


Figure 5.11: MATLAB Simulation 2: Adapting for \tilde{C}_2

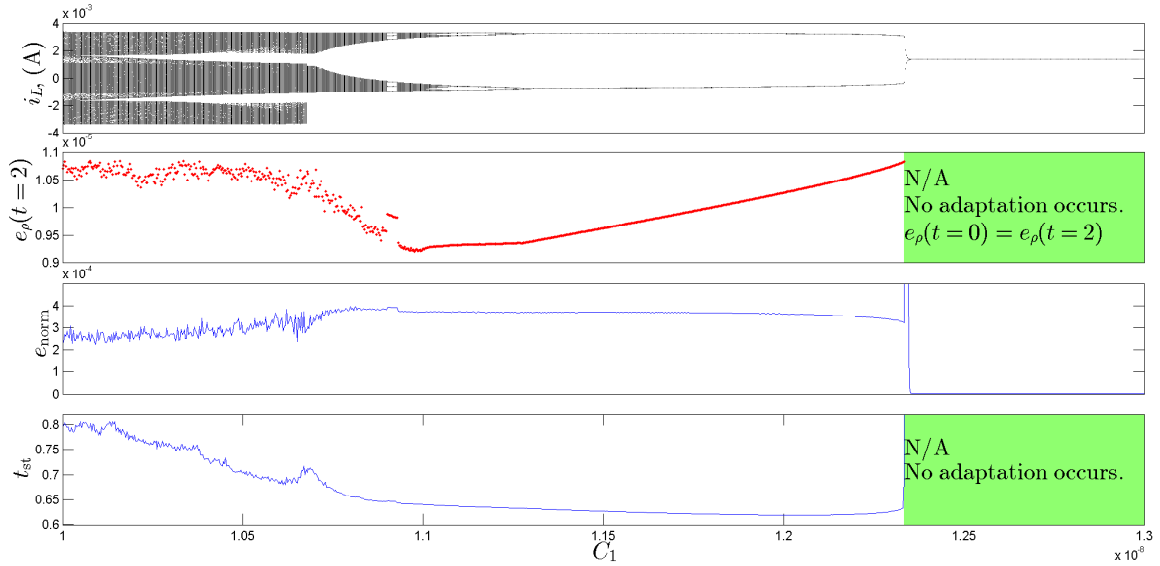


Figure 5.12: MATLAB Simulation 3: Adapting for \tilde{L} with tolerances.

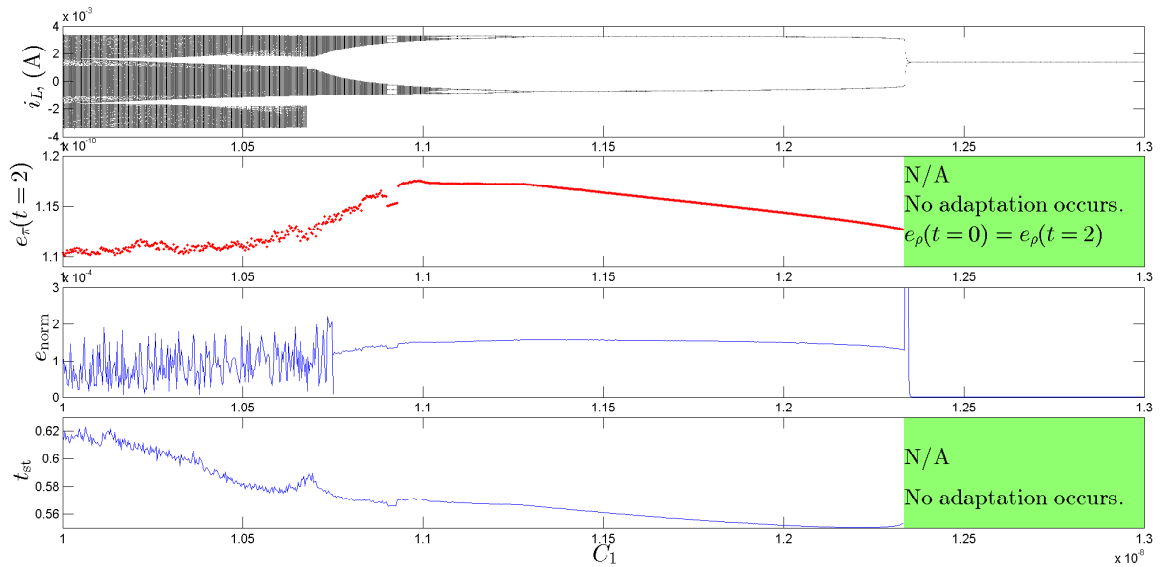


Figure 5.13: MATLAB Simulation 4: Adapting for \tilde{C}_2 with tolerances.

5.4 Discussion

We begin by comparing Experiment 1, SPICE Simulation 1, and SPICE Simulation 2. The experiment and simulations each use the same adaptive controller. Two differences are observed between the experiment and simulation. First, we contrast the fluctuation in R_0 (and \tilde{R}_0) for the experiment versus simulation. In each case, we use $R_0 = \tilde{R}_0 = 200 \Omega$. However, the least square estimates yield

$R_{0\text{est}} \cong \tilde{R}_{0\text{est}} \cong 226 \Omega$ for the experiment, $R_{0\text{est}} \cong \tilde{R}_{0\text{est}} \cong 202 \Omega$ for SPICE Simulation 1, and $R_{0\text{est}} = \tilde{R}_{0\text{est}} \cong 203 \Omega$ for SPICE Simulation 2. The large deviation in the resistance estimates for the experimental data can be ascribed to the unmodeled parasitic effects of the inductor-gyrator. For more details on the parasitic effects arising due to CFOA see [Kacar and Kuntman, 2011]. Second, the ideal value of L using (4.9), resulting from the ideal CFOA model, can be shown to be 40.5 mH. However, the least square estimates yield $L_{\text{est}} = 50.8$ mH for the experiment and $L_{\text{est}} = 45.4$ mH for SPICE Simulations 1 and 2. Once again, the differences in the least square estimates of L *vis-à-vis* the ideal L can be ascribed to the parasitic effects neglected by the ideal model.

Next, note that in SPICE Simulation 1, the least square estimates of L and \tilde{L} are virtually the same, indicating convergence of adaptive parameter to the actual parameter value. In contrast, in the case of the experimental data and SPICE Simulation 2 data, the least square estimates of \tilde{L} are offset from the estimate of L by approximately 1 mH in Experiment 1 and 0.1 mH in SPICE Simulation 2. In a simulation study of adaptive synchronization of Chua's oscillators with a mismatched parameter, Parlitz and Kocarev [1996] similarly observed that the adaptive parameter converges to a value slightly offset from the desired value.

Experiment 4, SPICE Simulation 3, and SPICE Simulation 4 are comparable to Experiment 1, SPICE Simulation 1, and SPICE Simulation 2, respectively. However in the case of Experiment 4, SPICE Simulation 3, and SPICE Simulation 4, the master Chua's attractor is purposefully designed to yield simple oscillations instead of chaotic oscillations. That is, in this case the conditions for PE are no longer met according to Lian et al. [2002]. Note that, in this case, Theorem 1 guarantees state synchronization and parameter convergence to some constant. However, since the series connection of R_0 and L (alternatively \tilde{R}_0 and \tilde{L}) is a first order system and e_{v_2} and e_{i_L} converge to zero, it follows that $\lim_{t \rightarrow \infty} \tilde{L}(t) \rightarrow L$.

Next, we contrast the results of MATLAB Simulations 1–4. Note that MATLAB Simulations 1 and 2 correspond to the ideal case and if these are allowed to run for longer than two seconds, the values for e_{norm} , e_π , e_ρ will asymptotically decrease to zero. In contrast, MATLAB Simulations 3 and 4 demonstrate the behavior observed in Experiment 1 and SPICE Simulation 2 wherein the adaptive parameter continues to oscillate around a value that has a slight offset from the actual parameter value. In MATLAB Simulations 1–4, we note that as C_1 changes the trend for the measure t_{st} is the same for all simulations. As C_1 changes from 1 nF to 1.3 nF the master Chua's circuit goes from chaos to equilibrium. Note the large spikes on e_{norm} at around $C_1 = 12.32$ nF. These spikes are due to the fact that in this small range of C_1 the Chua's oscillator is approaching equilibrium very slowly in which the 2 second simulation time is not enough for the master Chua's oscillator to reach its steady state behavior. The only time e_{norm} reaches close to zero is when the Chua's attractor is in equilibrium, which is when C_1 goes above 12.33 nF. At equilibrium, the energy storing components no longer have a long term effect on the system and the inductor functionally behaves as a short and the capacitors behave as open. In this mode, the adaptive parameters do not converge to any particular value but stay the same. Note that, this would not be the case for adapting resistive parameters such as R_0 .

Consider that the mismatched parameters are R_0 and \tilde{R}_0 . In this case, new error dynamics can

be derived as in (3.2) and (3.18). Next, using the same Lyapunov-based technique as in Chapter 3 with a candidate Lyapunov function

$$V(e_{v_1}, e_{v_2}, e_{i_L}, e_\rho) = \frac{C_1}{4} e_{v_1}^2 + \frac{C_2}{2} e_{v_2}^2 + \frac{L}{2} e_{i_L}^2 + \frac{1}{2\psi} e_\phi^2, \quad (5.1)$$

where $e_\phi = \tilde{R}_0 - R_0$, we can achieve a similar stability result by using controller (3.3), applying condition (3.5), and using the parameter update law

$$\frac{d}{dt} (\tilde{R}_0) = \psi e_{i_L} (\tilde{i}_L), \quad (5.2)$$

where ψ is a positive constant. For this case, we will have parameter matching of R_0 and \tilde{R}_0 even in the DC case. Assume that we have full control of C_1 to change the master Chua's oscillator behavior and have a mismatch of one resistive parameter and one energy storing parameters (such as $\tilde{R}_0 \neq R_0$ and $\tilde{L} \neq L$). In this case, we suggest the following adaptive parameter tuning methodology.

1. Set C_1 to bring the master Chua's oscillator to a steady state.
2. Adapt \tilde{R}_0 until parameter converges.
3. Stop adapting \tilde{R}_0 . Change C_1 to bring the master Chua's oscillator to a bounded orbit.
4. Adapt \tilde{L} until parameter converges.

This algorithm is applied in a MATLAB simulation for the case when $L = 0.018$ mH, $\tilde{L}(t=0) = 0.010$ mH, $R_0 = 13 \Omega$, $\tilde{R}_0(t=0) = 10 \Omega$. During step (1) C_1 is set to 13 nF @ $t = 0$ s. Step (2) is initiated @ $t = 0.5$ s, for step (3) C_1 is set to 10 nF @ $t = 2$ s, and step (4) is initiated @ $t = 2.5$ s. Results are shown in Figure 5.14, which displays the state i_L of the master Chua's oscillator, and parameters L , \tilde{L} , R_0 , and \tilde{R}_0 .

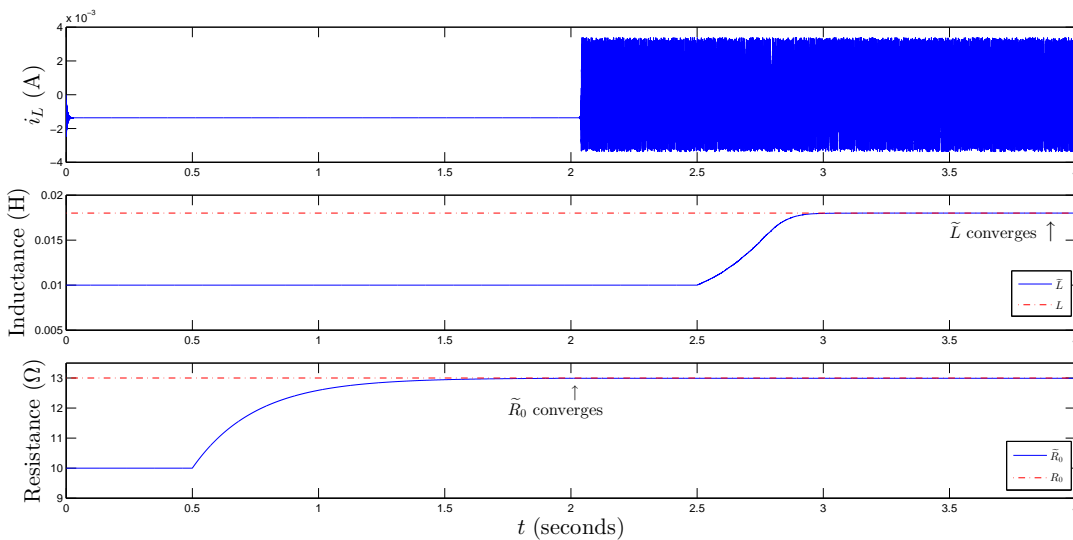


Figure 5.14: Demonstration of four step tuning methodology.

Chapter 6

Conclusion

In this research, we presented two adaptive controllers that are designed to match a parameter (L or C_2) in two Chua's circuits with the presence of PE. We implemented one of the adaptive controllers using analog circuitry. To our knowledge, this is the first instance of adaptive synchronization with parameter matching wherein the Chua's oscillators and adaptive controller are realized using analog circuits. We have also shown SPICE simulations analogous to our experimental results. Furthermore we tested our two adaptive controllers over many conditions of the Chua's oscillator in MATLAB. Our results show that the adaptive controller achieves parameter matching while the system is chaotic, but also when the system is a simple oscillator (and does not fulfill the qualities of PE). Finally we outlined conditions under which parameter matching can be achieved even when the master Chua's oscillator is at equilibrium.

Appendix A

TINA-TI SPICE Simulation 1 Schematic

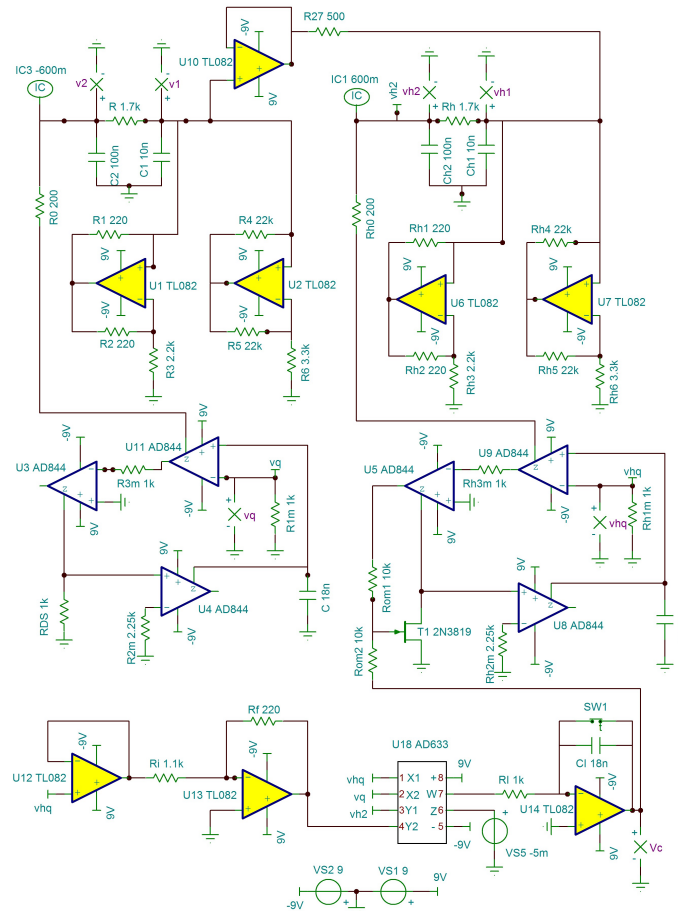


Figure A.1: TINA-TI Schematic of SPICE Simulation 1.

Appendix B

MATLAB-Simulink Simulation

B.1 MATLAB-Simulink

The MATLAB-Simulink simulations mentioned in Section 5.3 are described below, we will use MATLAB Simulation 2 as our example. A MATLAB script (“Run.m”) sweeps through a certain number of values of parameter C_1 , and calls a Simulink model (“Adapte_Synch_C2_IdealChua.mdl”) for every value of C_1 . The Simulink model returns the necessary data back to the MATLAB script which is saved in a .MAT file. The results of 1,000 simulations are generated by distributing the task between four computers. The sections below will show the MATLAB files and Simulink models used to generate the data for MATLAB Simulation 2.

B.1.1 Run.m

```
%*****C2 Tuning*****  
clc  
clear  
close all  
Adapt_Synch_C2_prep  
  
figure (1);  
xlabel('C1')  
ylabel('eC2')  
hold on  
figure (2);  
xlabel('C1')  
ylabel('e_norm')  
hold on  
figure (3);  
xlabel('C1')  
ylabel('t_st')
```

```

hold on

C2 = 100*10(-9);

%stepsize = 0.00001;
%time is 1 second

Clinc = 0.7500;
PCnum = 1;

C1_min = (10+Clinc*(PCnum-1))*10(-9);
C1_max = (10+Clinc*PCnum)*10(-9);
K = 250;
i_d = 1;

time = 2;
stepsize = 0.00001;

eLVec = zeros(K,1);
Clvec = zeros(K,1);
eVec = zeros(K,1);
tsVec = zeros(K,1);
for k = 1:K
    C1 = C1_min + (k-1)*(C1_max-C1_min)/(K-1);
    Clvec(k) = C1;

    [T2,X2, Y2] = sim('Adapt_Synch_C2_IdealChua');
    eC2 = abs(Y2(end,4)-C2);
    eC2Vec(k) = eC2;

    e = norm(Y2(end,1:3),2);
    eVec(k) = e;

    I = find(abs((Y2(:,4)-C2))./C2 < 0.1,1,'first');
    if isempty(I)
        I = length(T2);
    end
    tsVec(k) = T2(I);
    figure(1)
    plot(C1,eC2,'.','MarkerSize',5,'Color','red')
    figure(2)
    plot(C1,e,'.','MarkerSize',5,'Color','blue')
    figure(3)
    plot(C1,T2(I),'.','MarkerSize',5,'Color','blue')
end
save('eC2Vec','eC2Vec') % the normalized perportion of Lhat final, to L
save('Clvec','Clvec') % the values of L used
save('eVec','eVec') %the normalized value of the e_x, e_y and e_z
save('tsVec','tsVec')%the time it took for Lhat to reach settling time 1%

```

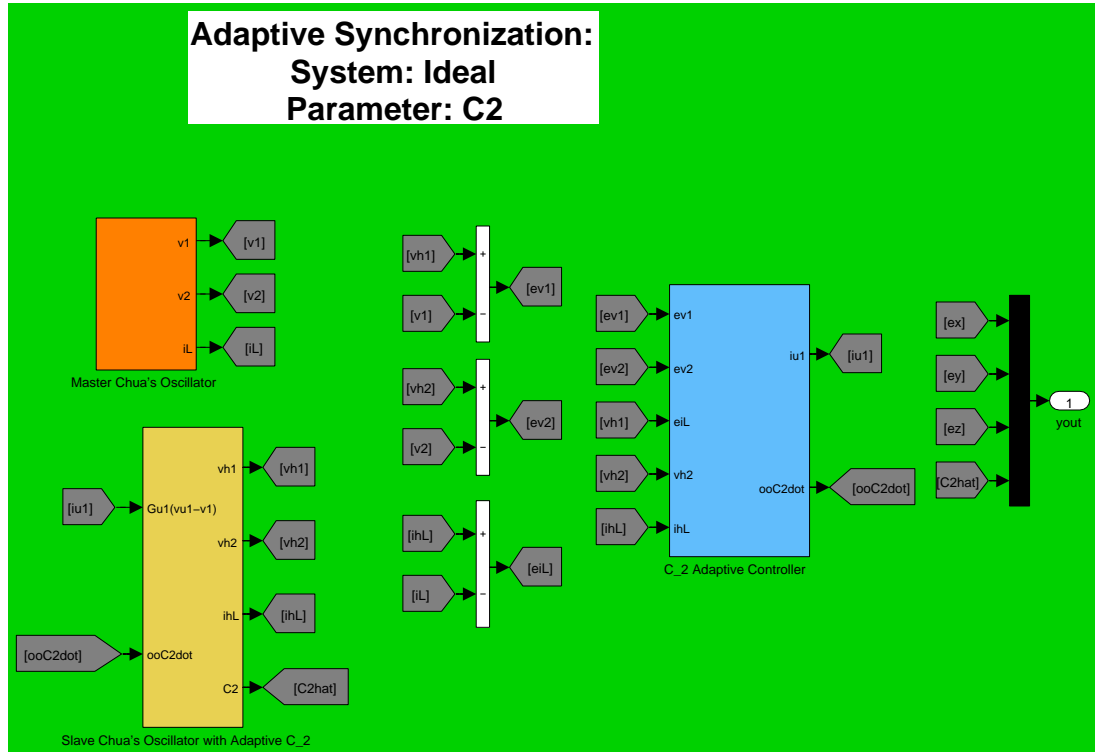



Figure B.1: Simulink model Adapte_Synch_C2_IdealChua.mdl.

B.2 Master Chua's Oscillator

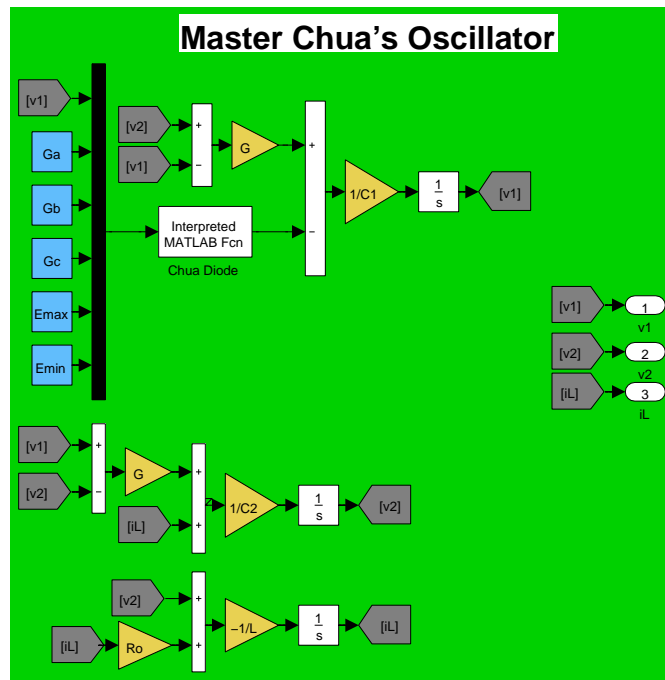


Figure B.2: Simulink model of master Chua's oscillator.

B.3 Slave Chua's Oscillator

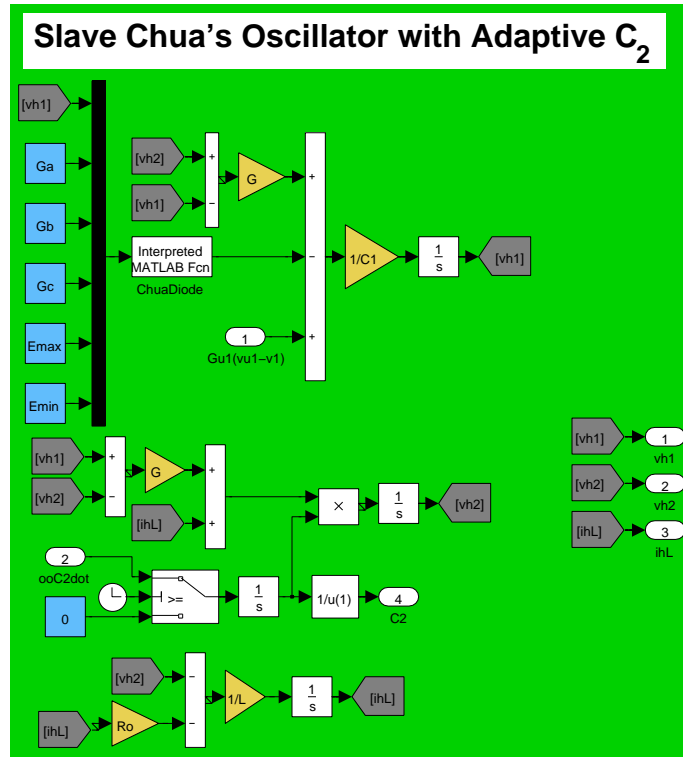


Figure B.3: Simulink model of slave Chua's oscillator with adaptive C_2 .

B.3.1 C_2 Adaptive Controller

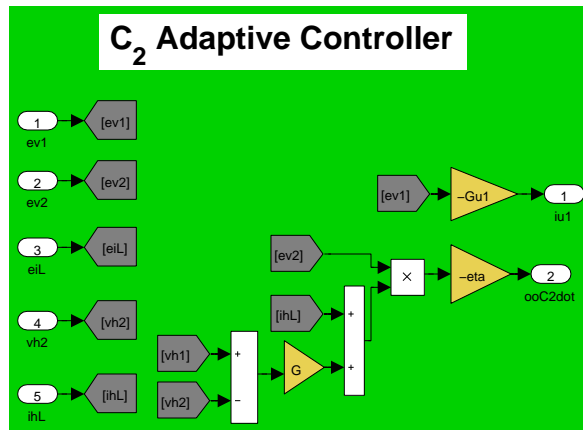


Figure B.4: Simulink Model of C_2 Adaptive Controller.

B.3.2 Chua Diode

```

%ChuaDiode.m
function o = ChuaDiode(i)

x = i(1);
Ga = i(2);
Gb = i(3);
Gc = i(4);
Emax = i(5);
Emin = i(6);

if abs(x) < Emin
    o = x*Ga;

elseif abs(x) >= Emin
    o = x*Gb;
    if x > 0
        o = o + Emin*(Ga-Gb);
    else
        o = o + Emin*(Gb-Ga);
    end
end
%end ChuaDiode.m

```

B.4 Bifurcation

B.4.1 BifurcationAnalysis.m

```

%BifurcationAnalysis.m
%This code generates data necessary for the file BifurcationPlot.m
%to create a bifurcation diagram for the Chua's oscillator by sweeping the
%parameter C1 and collecting all the points that pass through plain Sigma,
%which intersects the system's equilibrium points.

%Note: This file is meant to be copied between four PCs to distribute
%the computational load. The variable PCnum indicates which portion of the
%bifurcation data to generate.

clc
clear all
close all
Chua_prep %loads the prep file for Chua.mdl
figure (1)
hold on

%stepsize = 0.00001;
%time is 1 second;

```

```

Clinc = 0.7500;
PCnum = 1; %Change PC number accordingly [1-4]

Cl_min = (10+Clinc*(PCnum-1))*10^(-9);
Cl_max = (10+Clinc*PCnum)*10^(-9);
K = 250;

%Allocating Memory
Data = zeros((1/stepsize) + 2 ,K*2);
Clvec = zeros(K,1);
for k = 1:K

    C1 = Cl_min + (k-1)*(Cl_max-Cl_min)/(K-1); %Change C1 value
    Clvec(k) = C1;
    [T,X,Y]= sim('Chua'); %run Simulink simulation
    Data(:,(k*2-1):k*2) = Y; %Save the necessary data from Simulink

    % Hint: m = y/z b = 0
    %   y = -0.017773051800091
    %   z = 0.001367157830776

    l_Y = length(Y);
    %Index of the last 10% of points that intersect the plane Sigma
    I = find(Y(floor(l_Y*0.9):end,2)>0)+floor(l_Y*0.9)-1;
    l_I = length(I);
    plot(C1*ones(l_I,1),Y(I,1),'.') %Plot to see progress.
end
save('Data','Data')
save('Clvec','Clvec')
BifurcationPlot
hold off

```

B.4.2 Simulink Diagram Called by BifurcationAnalysis.m

Chua Oscillator with Bifurcation Data Output

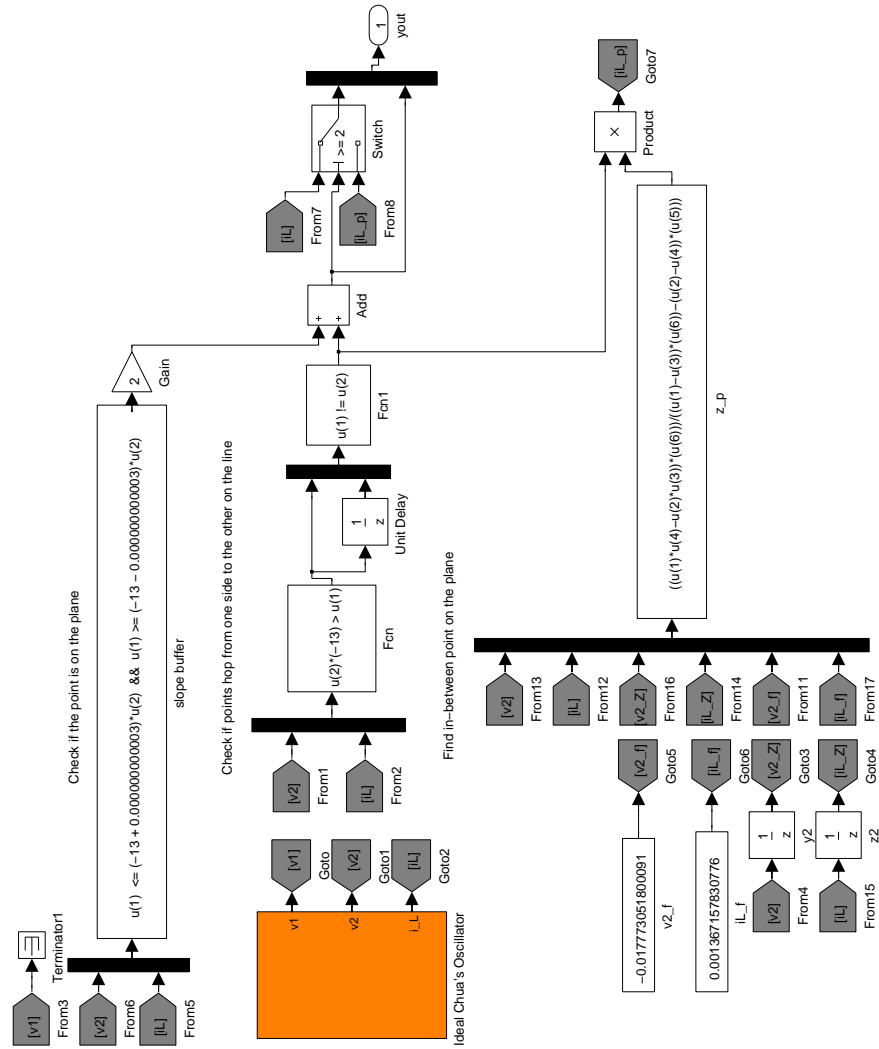


Figure B.5: Simulink model used to generate bifurcation data.

Bibliography

- T. Aida and P. Davis. Oscillation mode selection using bifurcation of chaotic mode transitions in a nonlinear ring resonator. *IEEE J. Quantum Electron.*, 30(12):2986–2997, 1994.
- AnalogDevices. AD633 analog multiplier macro model, 2013a.
- AnalogDevices. AD844 monolithic op amp macro model, 2013b.
- S. Bowong, M. Kakmeni, and R. Koina. Chaos synchronization and duration time of a class of uncertain chaotic systems. *Math. Comput. Simul.*, 71(3):212 – 228, 2006.
- R. Brown, L. Chua, and B. Popp. Is sensitive dependence on initial conditions natures sensory device? *Int. J. Biurcat. Chaos*, 2(1):193–199, 1992.
- L. O. Chua. Chua's circuit: An overview ten years later. *J. Circuit. Syst. Comp.*, 4(2):117–159, 1994.
- L. O. Chua, L. Kocarev, K. Eckert, and M. Itoh. Experimental chaos synchronization in Chua's circuit. *Int. J. Biurcat. Chaos*, 2(3):705–708, 1992.
- L. O. Chua, T. Yang, G.-Q. Zhong, and C. W. Wu. Adaptive synchronization of Chua's oscillators. *Int. J. Biurcat. Chaos*, 6(1):189–201, 1996.
- A. B. Cohen, B. Ravoori, F. Sorrentino, T. E. Murphy, E. Ott, and R. Roy. Dynamic synchronization of a time-evolving optical network of chaotic oscillators. *Chaos*, 20(4):043142, 2010.
- N. J. Corron and D. W. Hahs. A new approach to communications using chaotic signals. *IEEE Trans. Circuits Syst. I, Fundam. Theory Appl*, 44(5):373–382, 1997.
- J. Cruz and L. Chua. An IC chip of Chua's circuit. *IEEE Trans. Circuits Syst. II, Analog Digit. Signal Process.*, 40(10):614 –625, oct 1993.
- C. Dubey and V. Kapila. Wave fractal dimension as a tool in detecting cracks in beam structures. *Chaotic Modeling and Simulation (CMSIM)*, 1(2):241–256, 2012. ISSN 2241-0503.
- R. Femat, J. Alvarez-Ramrez, and G. Fernandez-Anaya. Adaptive synchronization of high-order chaotic systems: a feedback with low-order parametrization. *PHYSICA D*, 139(34):231 – 246, 2000. ISSN 0167-2789.

- A. Fradkov and A. Markov. Adaptive synchronization of chaotic systems based on speed gradient method and passification. *IEEE Trans. Circuits Syst. I, Fundam. Theory Appl*, 44(10):905–912, oct 1997.
- A. Fradkov, H. Nijmeijer, and A. Markov. Adaptive observer-based synchronization for communication. *Int. J. Biurcat. Chaos*, 10(12):2807–2813, 2000.
- S. Ge and C. Wang. Adaptive control of uncertain Chua’s circuits. *IEEE Trans. Circuits Syst. I, Fundam. Theory Appl*, 47(9):1397–1402, 2000.
- Z. Ge and T. Lin. Chaos, chaos control and synchronization of electro-mechanical gyrostat system. *J. Sound Vibration*, 259(3):585–603, 2003.
- M. Haeri and B. Khademian. Comparison between different synchronization methods of identical chaotic systems. *Chaos Soliton. Fract.*, 29(4):1002 – 1022, 2006.
- A. Hegazi, H. Agiza, and M. El-Dessoky. Adaptive synchronization for Rössler and Chua’s circuit systems. *Int. J. Biurcat. Chaos*, 12(7):1579–1597, 2002.
- B. Huberman and E. Lumer. Dynamics of adaptive systems. *IEEE Trans. Circuits Syst. I, Reg. Papers*, 37(4):547–550, apr 1990.
- X.-Z. Jin, W. wei Che, and D. Wang. Adaptive synchronization of uncertain and delayed chaotic systems with its circuit realization. In *Intelligent Control and Automation (WCICA), 2012 10th World Congress on*, pages 3465–3470, july 2012.
- J. K. John and R. Amritkar. Synchronization by feedback and adaptive control. *Int. J. Biurcat. Chaos*, 4(6):1687–1695, 1994.
- F. Kacar and H. Kuntman. CFOA-based lossless and lossy inductance simulators. *Radioengineering*, 20(3):627–631, 2011.
- R. Kilic. *A Practical Guide for Studying Chua’s Circuits*. World Scientific Publishing Company, 2010.
- H. R. Koofgar, F. Sheikholeslam, and S. Hosseinnia. Robust adaptive synchronization for a general class of uncertain chaotic systems with application to Chua’s circuit. *Chaos*, 21(4):043134, 2011. ISSN 10541500.
- A. K. Kozlov, V. D. Shalfeev, and L. O. Chua. Exact synchronization of mismatched chaotic systems. *Int. J. Biurcat. Chaos*, 6(3):569–580, 1996.
- K.-Y. Lian, P. Liu, T.-S. Chiang, and C.-S. Chiu. Adaptive synchronization design for chaotic systems via a scalar driving signal. *IEEE Trans. Circuits Syst. I, Fundam. Theory Appl*, 49(1):17–27, jan 2002.
- J. Lin, T. Liao, J. Yan, and H. Yau. Synchronization of unidirectional coupled chaotic systems with unknown channel time-delay: Adaptive robust observer-based approach. 26(3):971–978, 2005.
- X. Liu and T. Chen. Synchronization of identical neural networks and other systems with an adaptive coupling strength. *Int. J. Circ. Theor. App.*, 38(6):631–648, 2010.

- T. Matsumoto. A chaotic attractor from Chua's circuit. *IEEE Trans. Circuits Syst. I, Reg. Papers*, 31(12):1055–1058, december 1984.
- G. Mayer-Kress, I. Choi, N. Weber, R. Barger, and A. Hubler. Musical signals from Chua's circuit. *IEEE Trans. Circuits Syst. II, Analog Digit. Signal Process*, 40(10):688–695, oct 1993.
- K. Narendra and A. Annaswamy. *Stable adaptive systems*. Dover Publications, 2005.
- M. Naseh and M. Haeri. An adaptive approach to synchronization of two Chuas circuits. In *WEC'05: The Fourth World Enformatika Conference*. Citeseer, 2005.
- K. Nay and A. Budak. A voltage-controlled resistance with wide dynamic range and low distortion. *IEEE Trans. Circuits Syst. I, Reg. Papers*, 30(10):770–772, 1983.
- J. Nichols, S. Trickey, M. Todd, and L. Virgin. Structural health monitoring through chaotic interrogation. *Meccanica*, 38(2):239–250, 2003.
- U. Parlitz and L. Kocarev. Multichannel communication using autosynchronization. *Int. J. Bifurcat. Chaos*, 6(3):581–588, 1996.
- L. M. Pecora and T. L. Carroll. Synchronization in chaotic systems. *Phys. Rev. Lett.*, 64:821–824, Feb 1990.
- B. Ravoori, A. B. Cohen, A. V. Setty, F. Sorrentino, T. E. Murphy, E. Ott, and R. Roy. Adaptive synchronization of coupled chaotic oscillators. *Phys. Rev. E*, 80:056205, Nov 2009.
- A. Rodriguez-Vazquez and M. Delgado-Restituto. CMOS design of chaotic oscillators using state variables: a monolithic Chua's circuit. *IEEE Trans. Circuits Syst. II, Analog Digit. Signal Process.*, 40(10):596–613, oct 1993.
- S. Sastry and M. Bodson. *Adaptive control: stability, convergence and robustness*. Dover Publications, 2011.
- R. Senani. Realization of a class of analog signal processing/signal generation circuits: Novel configurations using current feedback op-amps. *Frequenz*, 52(9-10):196–206, 1998.
- R. Senani, D. R. Bhaskar, S. S. Gupta, and V. K. Singh. A configuration for realizing floating, linear, voltage-controlled resistance, inductance and FDNC elements. *Int. J. Circuit Theory Appl.*, 37(5), 2009.
- A. M. Soliman. Applications of the current feedback operational amplifiers. *Analog Integr. Circ. S.*, 11(3):265–302, 1996.
- TexasInstruments. Getting started with TINA-TI, 2008. URL <http://www.ti.com>.
- TexasInstruments. TL082 SPICE macro-model, 2013. URL <http://www.ti.com/product/tl082>.
- D. J. Wagg. Partial synchronization of nonidentical chaotic systems via adaptive control, with applications to modeling coupled nonlinear systems. *Int. J. Bifurcat. Chaos*, 12(3):561–570, 2002.
- C. Wu. *Synchronization in coupled chaotic circuits and systems*, volume 41. World Scientific Publishing Company Incorporated, 2002.

- C. W. Wu, T. Yang, and L. O. Chua. On adaptive synchronization and control of nonlinear dynamical systems. *Int. J. Biurcat. Chaos*, 6(3):455–471, 1996.
- M. Xiao and J. Cao. Synchronization of a chaotic electronic circuit system with cubic term via adaptive feedback control. *Commun. Nonlinear Sci. Numer. Simul.*, 14(8):3379 – 3388, 2009. ISSN 1007-5704.
- Q. Xie, G. Chen, and E. Bollt. Hybrid chaos synchronization and its application in information processing. *Math. Comput. Modell.*, 35(12):145 – 163, 2002.
- G.-Q. Zhong, R. Bargar, and K. S. Halle. Circuits for voltage tuning the parameters of Chua’s circuit: Experimental application for musical signal generation. *J. Franklin Inst.*, 331(6):743 – 784, 1994.
- J. Zhou, T. Chen, and L. Xiang. Adaptive synchronization of coupled chaotic delayed systems based on parameter identification and its applications. *Int. J. Biurcat. Chaos*, 16(10):2923–2933, 2006.
- H. Zhu and B. Cui. A new adaptive synchronization scheme of delayed chaotic system for secure communication with channel noises. In *Computer Design and Applications (ICDDA), 2010 International Conference on*, volume 4, pages V4–433. IEEE, 2010.